FINAL REPORT
RESEARCH STUDIES USING OSO-6 ZODIACAL LIGHT EXPERIMENT DATA

PREPARED FOR:
NATIONAL AERONAUTICS AND SPACE ADMINISTRATION
HEADQUARTERS
CODE SL

BY:
MEASUREMENTS ANALYSIS CORPORATION
BOULDER, COLORADO

NOVEMBER, 1977

CONTRACT NO. NASW-2902

TABLE OF CONTENTS

SECTION	TITLE	PAGE
	FOREWORD	i
	TABLE OF CONTENTS	ii
	LIST OF ILLUSTRATIONS	iii
	INTRODUCTION	v
1.0	INSTRUMENT OPERATION AND ORBITAL CALIBRATION	1-1
	1.1 Major Instrument Functions and Orbital Performance	1-1
	1.2 Instrumental Corrections Applied to Data	1-5
	1.2.1 Thermal Effects	1-6
	1.2.2 System Gain	1-9
	1.2.3 System Degradation	1-10
	1.2.4 South Atlantic Anomaly Effects	1-13
	1.3 Instrument Color Characteristics	1-13
	1.4 Orientation of Observations on Sky	1-15
	1.5 Scattered Light	1-16
	1.6 Absolute Calibration	1-17
	1.6.2 Calibrations Using Ground-Based Milky Way and Zodiacal Light Information	1-23
	1.6.3 Integrated Calibration	1-24
2.0	ZODIACAL LIGHT VARIATION ANALYSIS	2-1
	2.1 Long Term Gegenschein Variation	2-1
	2.2 Evening/Morning Zodiacal Light Ratio	2-4
3.0	INTEGRATED STARLIGHT AND DIFFUSE GALACTIC LIGHT	3-1
4.0	EARTH/MOON LIBRATION REGION OBSERVATIONS	4-1
5.0	DATA PROCESSING	5-1
	5.1 New Orbits Processed	5-1
	5.2 Old Orbits Processed	5-3
	5.3 Analytical Processing	5-3
	5.4 Software/Data Formats/Tape Library	5-4
6.0	RECOMMENDATIONS	6-1
Appendix A	Zodiacal Light - Evening/Morning Ratios	A-1
Appendix B	On the Interstellar Dust Toward the Galactic Center	B-1
Appendix C	Data Processing Functional Flow and Software Programs	C-1

LIST OF ILLUSTRATIONS

FIGURE	TITLE	PAGE
1-1	Instrument Optical Schematic	1-2
1-2	Detector/Data Functional Schematic	1-4
1-3	Comparison of Basic Data History With Temperature Corrected History	1-8
1-4	Linearized and Degradation Corrected Data History	1-11
1-5	Effects of South Atlantic Anomaly on Data	1-12
1-6	Scattered Light Coefficients	1-19
1-7	Differentical Scattering Effect on Milky Way Color Index Determinations	1-20
1-8	Absolute Calibration in S_{10} Vis for Milky Way Crossing	1-25
1-9	Comparison of Milky Way Crossing Brightness with Ground Observations	1-26
1-10	Absolute Calibration in S_{10} Vis Using Milky Way Plus Star Crossings	1-28
1-11	Data History in Terms of S_{10} Vis	1-29
2-1	Comparison of Sky Background Brightness With Model And Resulting Residual Brightness	2-2
A-1	Comparison of Zodiacal Light Model with Three Cases	A-19
A-2	Illustration of Line of Sight of Zodiacal Light Observations	A-20
A-3	Correlation Plots of the Zodiacal Light Brightness	A-21
A-4	Correlation Plots of the Zodical Light Brightness	A-22
A-5	Polar Plot of Inverse Correlation Slope	A-23
A-6	Polar Plot of Evening/Morning Ratios	A-24
B-1	Mean Value of b-ŕ Index Versus Galactic Latitude	B-15
B-2	Isocolor Map in Galactic Latitude and Longitude	B-16
B-3	Mauna Kea Diffuse Galactic Light and OSO-6 Color Index	B-17

LIST OF ILLUSTRATIONS
(Continued)

FIGURE	TITLE	PAGE
B-4	Diffuse Galactic Light Versus OSO-6 b-r Index	B-18
B-5	Diffuse Galactic Light Index ϕ Versus OSO-6 b-r Index	B-19
B-6	The Quantity ϕ and Integrated Starlight Versus Galactic Latitude	B-20

TABLE

1-1	Comparison of OSO-6 Zodiacal Light Experiment Color Bands to Standard Astronomical Color Bands	1-14
1-2	Fractional Scattered Light Versus Angle From Line of Signt	1-18
1-3	Total Scattering for Various Sky Conditions	1-18
5-1	Data Processing Print Format	5-2
A-1	Hypothetical Cases of Zodiacal Light Errors	A-13
A-2	Comparison of Published Zodiacal Light Observations	A-14
A-3	Tabulation of Inverse Correlation Slope With Geocentric Latitude	A-15
B-1	Comparison of OSO-6 Color System With the Standard UBV System	B-12
B-2	Observed Color Index b-r	B-13
B-3	Diffuse Galactic Light Observed at Mauna Kea	B-14

INTRODUCTION

This report describes the results of the Research Studies on the OSO-6 Zodiacal Light Experiment, conducted by Measurements Analysis Corporation during the period from May 1976 to October 1977. Included in Section 1.0 is a discussion of the instrument performance and the empirical calibrations developed. Sections 2.0, 3.0, and 4.0 cover the three main areas of the research performed, i.e., (1) Zodiacal Light Variation Analysis; (2) Integrated Starlight and Diffuse Galactic Light; and (3) Earth/Moon Libration Region Counterglow. Considerable data processing has been performed during these studies and it is summarized in Section 5.0. Recommendations for future research to complete the interim results obtained, are given in Section 6.0.

1.0 INSTRUMENT OPERATION AND ORBITAL CALIBRATION

The OSO-6 Zodiacal Light Analyzer, ZLA, Experiment is a photo-polarimeter located in the rotating wheel section of the OSO spacecraft. OSO-6 was launched in August, 1969 and continued successuful operation until turned off in February, 1972. The ZLA experiment was developed for this mission by Rutgers University, under the direction of Dr. T. Rouy, Principal Investigator and assisted by Dr. B. Carroll, Rutgers, and Dr. L. Aller, UCLA, as Co-Investigators. Following the death of Dr. Rouy in 1969, these co-investigators were supplemented by two additional co-investigators, John Roach and Dr. F. E. Roach, and this team initiated analysis of the results coming in from the experiment. This analysis was complicated by the usual interpretation ambiguities of a major space experment, coupled with the loss of knowledge of much of the vital instrument characteristics as a result of Dr. Rouy's death. This co-investigator team spent considerable effort in the early analysis, establishing that much of the experiment data were useable, and that research analysis was warranted. Two of us (J. Roach and F. E. Roach) have continued this research under this contract and have defined the instrument in-orbit operational characteristics and have developed emperical calibrations, to the point where useable scientific results are being obtained. This section describes those characterictics and calibrations, which establish the validity of the scientific results from the experiment.

1.1 MAJOR INSTRUMENT FUNCTIONS AND ORBITAL PERFORMANCE

The OSO-6 ZLA has been described in several technical reports and will only be summarized here. An overall schematic is given in Figure 1-1, which shows the primary optics train culminating in the EMR-641 photomultiplier. The optics consist of the extended baffle tube, transmission lenses, the Rouey polarization prism and various transmission filters.

The f/1.6 objective lens system provided a field of view of 2 degrees. The baffle system was extended in orbit to provide rejection of light from outside this field of view from entering the telescope. It had

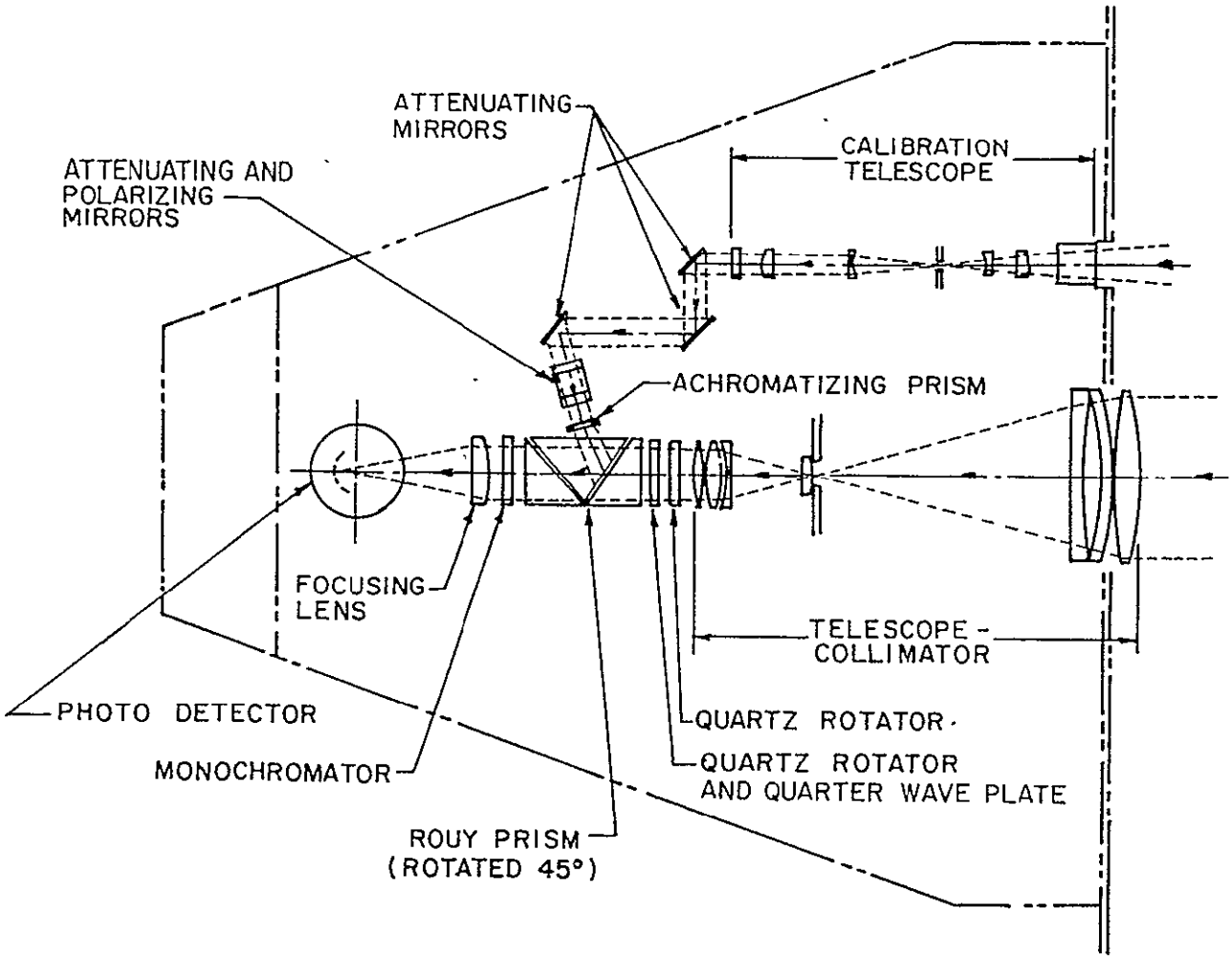
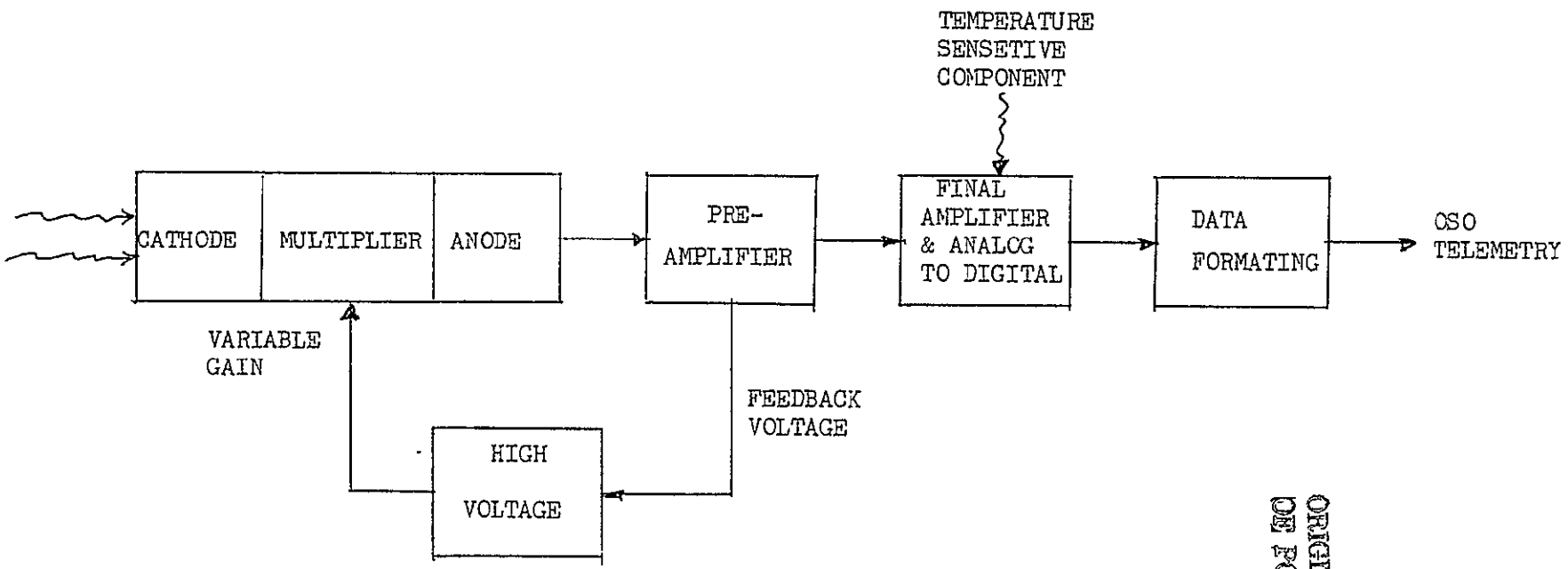


Figure 1-1 INSTRUMENT OPTICAL SCHEMATIC

a rejection coefficient, measured in orbit, of less than 10^{-4} at 10 degrees off axis. No part of the OSO structure was within 90 degrees of the entrance aperture. The light from the sky is collimated and passed through the bandpass filters, quartz rotators and the Rouy prism, and reimaged onto the photocathode.

A shutter closes off the telescope between each sky observation. It is opened by control of a series of sun sensors located around the periphery of the OSO wheel. These sensors provide signals that index observations every 5 degrees with respect to the Sun-OSO line. This sequence starts at satellite dawn at the elongation angle of 195 degrees; sequences through the anti-sun direction, around the sky; crosses the Sun; and finishes at elongation angle 195 degrees near the satellite dusk. The logic of the instrument counts each Sun sensor crossing (once per revolution or every 2 seconds) and sequences; (1) the shutter; (2) the bandpass filters; and (3) the quartz rotators. Each rotation of the wheel, three elongation angles are observed at one band and one polarization setting. This is repeated for five rotations and then the next band and polarization setting is made and so on until 90 observations are made for each of the three elongation angles. The next set of three elongation angles are started and the process continues until all observations are made; complete just before satellite dusk. These three mechanisms worked correctly throughout the 2 1/2 year mission, accumulating approximately 2.5×10^7 actuations. Dark current readings are made at the completion of the sequence just before dusk, with the shutter closed.

The EMR-641E photomultiplier is powered by a special slewing high voltage power supply in a closed loop system with the output preamplifier, as shown in Figure 1-2. As the incident light intensity increased, the amplifier output increases. This in turn decreased the high voltage which decreases the gain of the photomultiplier. This provides a logarithmic response for the system, over the range of expected Zodiacal light brightness. The system is linear until a minimum threshold brightness is reached. The photomultipler had an S-20 photocathode for good response across the three wavelength bands.



ORIGINAL PAGE IS
OF POOR QUALITY

Figure 1-2 DETECTOR/DATA FUNCTIONAL SCHEMATIC

Also shown in Figure 1-2 is the functional logic for the analog-to-digital converstion of the data and the final digital formating for transfer to the OSO telemetry. The data output is presented as 10 binary bits or with 1:1024 resolution. The status of the various operational elements of the instrument is multiplexed with the prime data before transfer to the telemetry. The temperature is multiplexed with the prime data before transfer to the telemetry. The temperature sensitive component, discussed in Section 1.2.1, is located in the analog-to-digital electronics, and thus affects only the output digital count. All other aspects of the electronics worked correctly throughout the lifetime of the experiment, except for occasional anomalies in some of the single bit status monitors. This required additional processing software logic to test for proper sequencing.

A direct Sun calibration optics train was incorporated in the instrument. However, the data from this system degraded dramatically early in the mission, probably due to radiation effects on the optics. Therefore no quantitative data have been processed from this system and all calibration work has been performed using the primary telescope, which was never exposed to direct sunlight.

The significant results form this experiment, discussed in later sections, are all based on data obtained within ±15 degrees of the anti-sun direction. This observing cone is obtained just after satellite dawn and just before satellite dusk. At these observing conditions the sunlit earth is greater than 90 degrees from the entrance aperture, and no extraneous light enters the telescope. However, as the OSO moves further into the orbital day, the sunlit earth is less than 90 degrees from the optical axis and the off axis scattered light swamps out the sky signal. Therefore, no useful data have been obtained from this experiment outside the anti-sun cone of elongation angles.

1.2 INSTRUMENTAL CORRECTIONS APPLIED TO DATA

The basic data telemetered from the instrument in the the OSO-6, include various instrumental effects that must be calibrated and corrected for in order to obtain useful scientific data. These include environmental effects as well as variable characteristics

in the instrument design. Considerable effort has been applied to calibrating these effects during this study and each area is discussed in detail.

1.2.1 Thermal Effects

This instrument was carefully designed to operate within the expected orbital thermal environment. However, two unexpected thermal effects on the instrument were encountered in orbit, that were not calibrated prior to launch. The first of these was a temperature sensitive component in the data output electronics that was not discovered until too late to replace it or calibrate it prior to launch. The second of these was the decrease in detector dark noise as a function of the lower operating temperature in orbit.

Temperature Sensitivity

The temperature sensitive component in the output amplifier of the data electronics (see Figure 1-2) became an extremely sensitive thermometer, as it caused variations in the output data count as a function of the instrument temperature. These variations were observed in the orbital data as the instrument temperature increased from the dawn to dusk observations; as it varied with the length of the day/night heating/cooling periods (related to the 51 day period of the ascending node); and as it varied as a function of the seasonal change in solar flux as the Earth's orbit varies in distance from the Sun. This variation in data count has an inverse correlation with temperature; i.e., the data count increased as the instrument temperature decreased.

The calibration correction for this effect has been determined from a cross section of data obtained at different intrument temperatures. There was no instrument temperature monitor near this sensitive electronic component. Therefore, we used as a temperature parameter the spacecraft hub temperature, which was the closest monitor to the instrument electronics. It also had the least sensitive temperature swing, and thus the most accurate protrayal of the probable instrument temperature.

We have applied this calibration to our complete 10,000 unit history. Shown in Figure 1-3 is the summary of this history for a constant sky background both as the uncorrected telemetry data, and the same data after the application of the temperature correction. The 51 day periodicity and the apehelion/perihelion variations are clearly evident in the top curve. In the corrected bottom curve, both of these effects have been removed and only the long term instrument degradation remains to be corrected.

In the actual telemetry data stream the hub temperature parameter is sampled every 24th data point taken from the sky. Therefore, in the data processing we have averaged the hub temperature data for the complete set of 540 sky readings for each dawn and dusk sequence, or an average over about 22 hub temperature samples. This has resulted in a consistent calibration parameter for this major instrument correction.

Dark Current

The dark current for the detector was calibrated only for the system operating at room temperature. This ground calibration showed a variation from 80 to 100 telemetry data counts for the high voltage readings encountered in most of the orbital data. However, since the instrument was operating at a lower temperature throughout most of its orbital history the actual "in orbit" dark current data count was probably significantly lower. The manufacturer's data for the type of photomultiplier used shows a decrease in dark current of about an order of magnitude from the room temperature operation to the nominal 15°C "in orbit" operation. Therefore, we have concluded that the actual dark current data count is a relatively small correction and no explicit correction alogrithm was applied to the data.

In the final processing two subtraction terms are applied to the data, which include a factor for the dark current term. These are the intercept term of the component correction algorithm and the intercept term of the final calibration conversion from linear data counts to physical units. Thus, any detector dark current contribution to the data has probably been corrected for in the processing algorithms used.

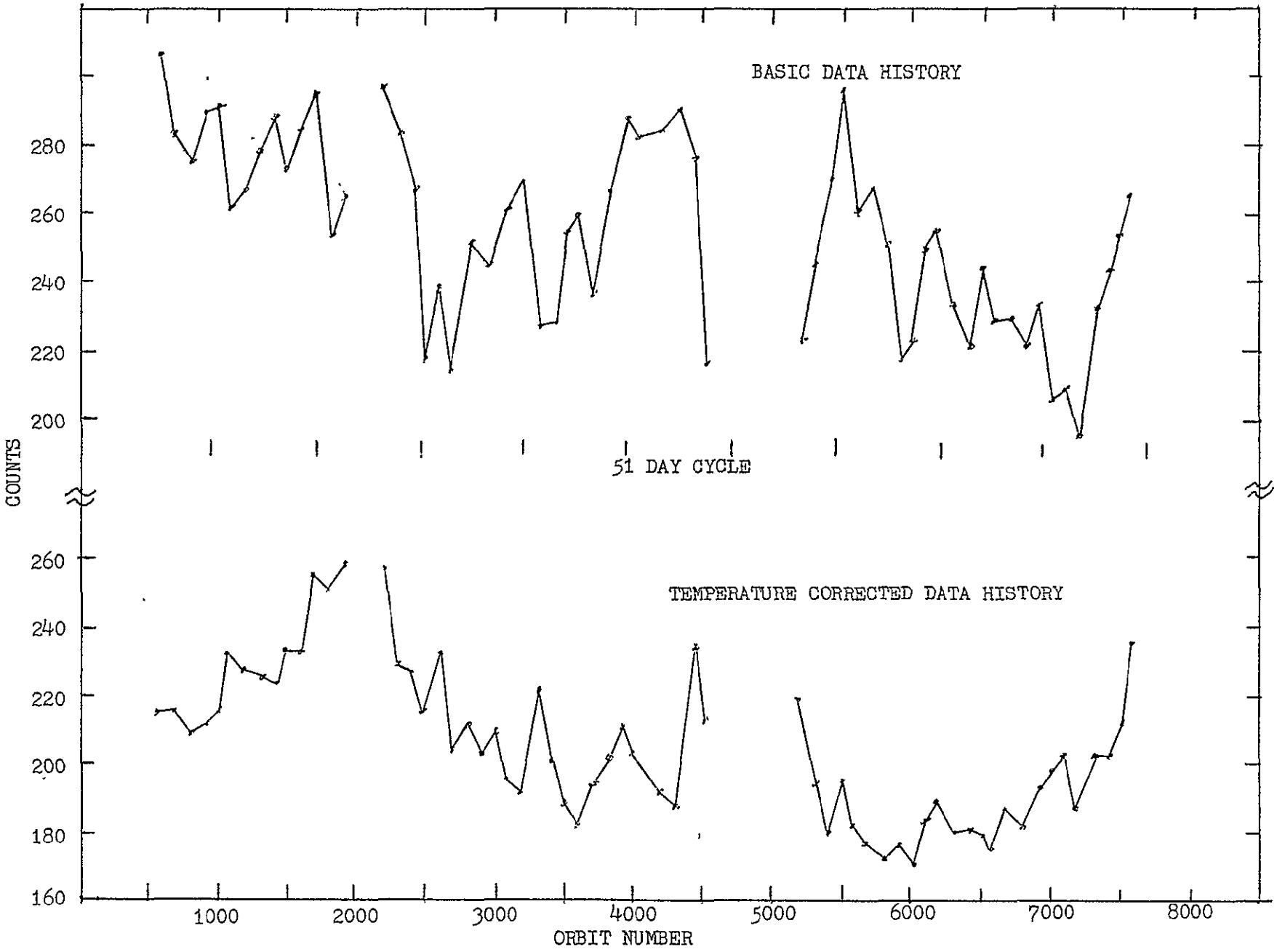


Figure 1-3 COMPARISON OF BASIC DATA HISTORY WITH TEMPERATURE CORRECTED DATA HISTORY

1.2.2 System Gain

The instrument was designed for a wide variation of sky signal, using a continuously variable photomultiplier gain system. This is shown in Figure 1-2 as a feedback from the pre-amplifer to the high voltage driving the photomultiplier. The effect of this feedback is: as the signal from the anode increased due to a brighter sky, the high voltage is reduced causing a lower gain. Thus the dynamic range of the instrument is increased to five decades of sky brightness over the 10 bit data word (1024 output counts).

This high voltage slewing is restricted at the low brightness end and doesn't come into effect until a threshold is reached, nominally a brightness greater than the gegenschein plus integrated starlight sky background.

The determination of the gain algorithm has been a major analytical effort during this study, due to its major effect on the conversion from the 10 bit telemetered data to the final linear data count. Starting with the latest ground calibration, taken about one year prior to launch, we have iterated several algorithms to determine the best fit to observed sky phenomena. This is best explained by noting that a bright star observation may have a data signature that is within the slewing range for the 5000 Å data, but within the non-slewing range for the 4000 Å and 6100 Å data. We have examined several star crossings of known spectral types and iterated the gain algorithm until a consistent set of color indices were obtained.

The result of this iterative analysis is that we have selected an algorithm that has a set point of bias at a slightly lower high voltage than the pre-launch calibration; that is, 2850 volts rather than 2974 volts. This means that the final linear data counts equal the telemetry data counts until a value of 242 counts is reached. Above this count level the slewing is in effect and we have used the pre-launch calibration slope alogrithm for conversion. The complete

algorithm used for the slewing region is:

$$\text{Linear Data Count} = \frac{\text{Telemetered Data Count (TDC)}}{\text{Gain}}$$

where: $\text{Gain} = \left(\frac{\text{High Voltage}}{2850}\right) \text{ Exp } 9.009$

and: $\text{High Voltage} = 3{,}224 - 1.545 \times \text{TDC}$

Note: $\text{Gain} = 1 \text{ for TDC} < 242 \text{ counts}$

This small adjustment in the "in orbit" value for the set point versus the final calibration taken over one year before launch, is probably due to continued aging of the photomultipler and/or a change due to derating of the electronics for "in orbit" operation.

Note that the history data in Figure 1-3 fall below the slewing range (242 counts) for the major part of the sky background. Therefore, the data effected by this algorithm are the brighter portions of the Milky Way and the bright star crossings. The Figure 1-3 data are then also the final linear data counts for the average sky background data.

1.2.3 System Degradation

As with any space instrument a continuous degradation was observed in this instrument throughout its orbital history. We determined this degradation factor empirically by comparing the same sky background data one year apart. Analyzing a series of these comparisons over the 2½ year history we established the following degradation corrections:

$$L(4000\ \text{Å}) : e^{0.000015(\text{Orbit Number})}$$
$$L(5000\ \text{Å}) : e^{0.000035(\text{Orbit Number})}$$
$$L(6100\ \text{Å}) : e^{0.000015(\text{Orbit Number}}$$

Applying these factors to the history data of Figure 1-3 we get the corrected linear data given in Figure 1-4. Comparison of the same sky background one year apart (5550 orbits) in Figure 1-4 shows this correction.

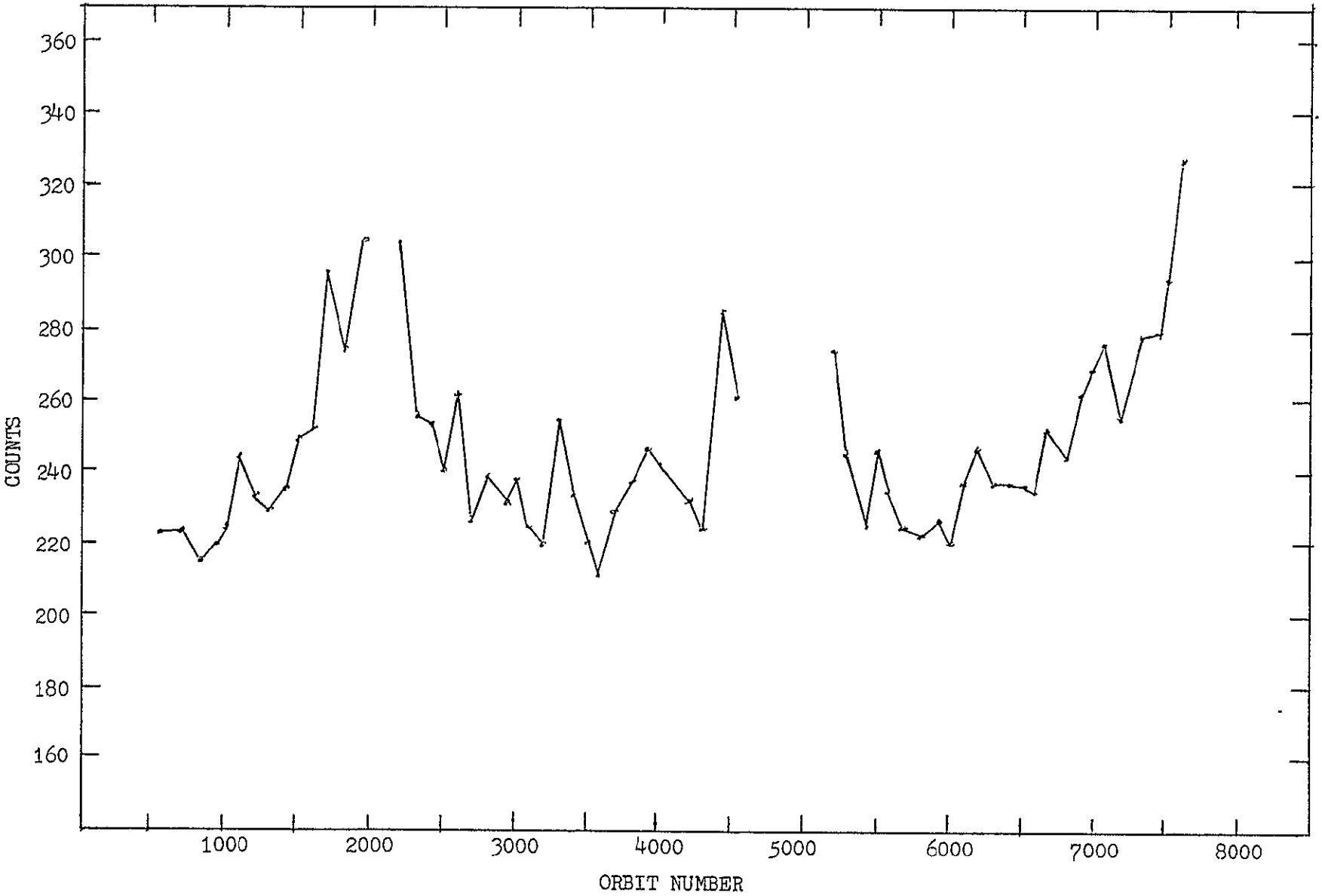


Figure 1-4 LINEARIZED AND DEGRADATION CORREDTED DATA HISTORY

This system degradation is primarily due to the continuous aging process of the photomultiplier in the space environment. Since there is a differential correction for the three colors some of the degradation must be due to aging of the optical filter material, which is the major component that is color unique. The degrading effect of the space radiation environment has been well established, both for the filter material and for the photomultiplier cathode.

1.2.4 South Atlantic Anomaly Effects

The photomultiplier of this instrument is sensitive to the radiation environment in Earth's orbit. The major effect seen is the increase in counts when the OSO-6 passed through the South Atlantic Anomaly (SAA). When passing near the center of the Anomaly the increase in counts is quite significant, as shown in Figure 1-5. These data spikes occur periodically during the history as the fixed anti-sun orientation precesses around the Earth, and crosses the center of the SAA every 15 orbits for a period of several hundred orbits.

This perturbation simply adds counts to the sky background counts. To remove this effect we underdraw the excess during analysis. We have not attempted to automate this correction, since its occurence is relatively infrequent in terms of the total history.

1.3 INSTRUMENT COLOR CHARACTERISTICS

The three wavelength bands in the OSO-6 instrument provide color index data for the sky background and objects observed. The correlation of the instrument wavelengths with those used for standard astronomical color indices is given in Table 1-1. In order to determine the instrumental characteristics for each of these bands, we have analyzed the data for various stars with well established color signatures. Adding to this analysis, the assumption that the average gegenshein plus integrated sky background is approximately the color of the sun we have established the instrument color constants. For

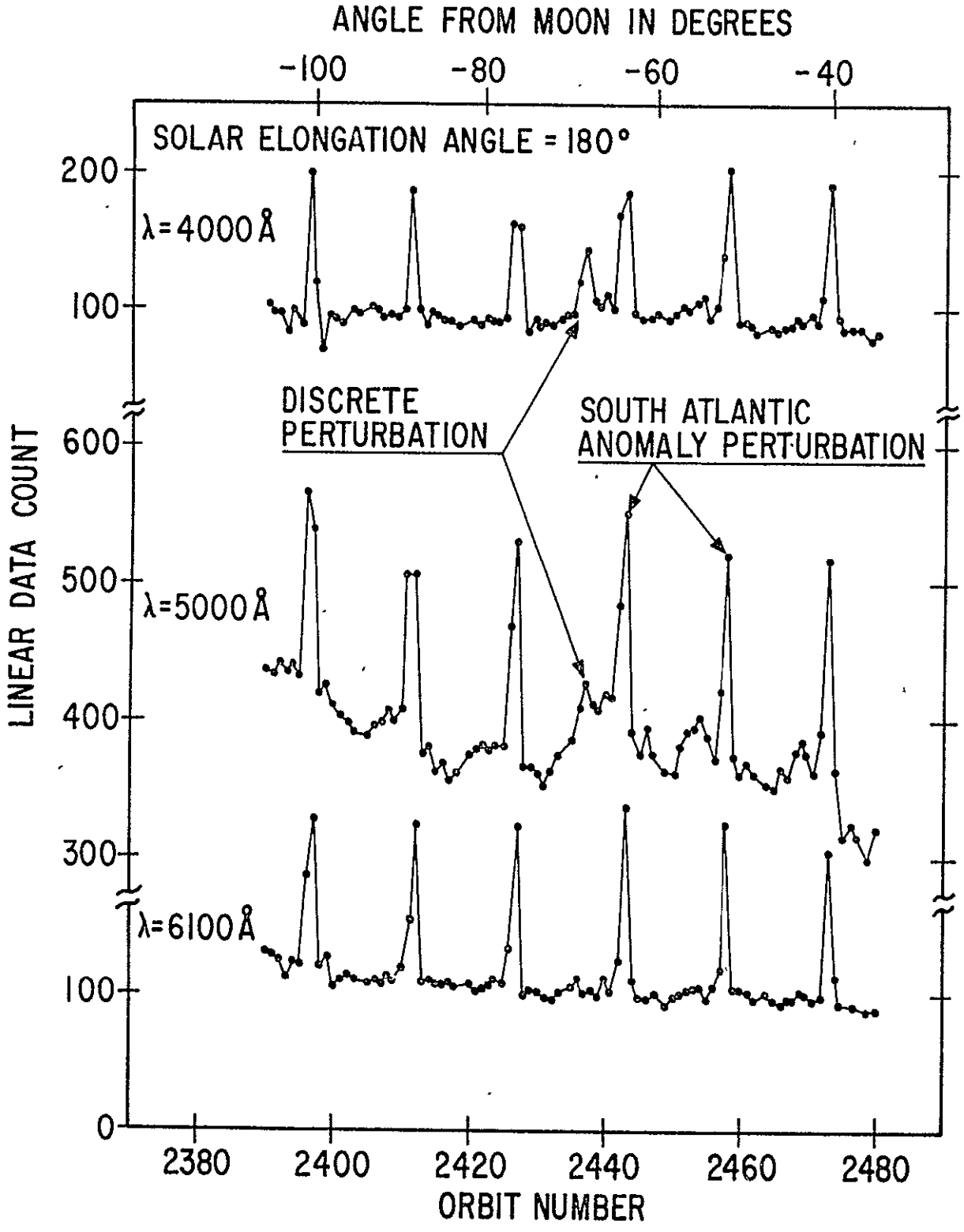


Figure 1-5 EFFECTS OF SOUTH ATLANTIC ANOMALY ON DATA

Table 1-1

COMPARISON OF OSO-6 ZODIACAL LIGHT EXPERIMENT COLOR BAND TO STANDARD ASTRONOMICAL COLOR BANDS

Astronomical	OSO-6	Peak Wavelength Angstroms
U		3500
	b	4000
B		4400
	v	5000
V		5500
	r	6100
R		7000

the three instrument color indices the preliminary algorithms are:

$$b\text{-}v = 2.5 \log \frac{L4000}{L5000} - k_1 \; ; \text{ where } k_1 = -0.184$$

$$b\text{-}r = 2.5 \log \frac{L4000}{L6100} - k_2 \; ; \text{ where } k_2 = +0.952$$

$$v\text{-}r = 2.5 \log \frac{L5000}{L6100} - k_3 \; ; \text{ where } k_3 = +1.136$$

We consider these constants as preliminary pending more detailed analysis of additional stars. This will improve the statistics and reduce the probable error for the constants. We have calculated these indices for the complete history as well as the sky temperature based on each index. The sky temperatures were calculated assuming black body relationships.

1.4 ORIENTATION OF OBSERVATIONS ON THE SKY

The optical axis of the instrument lies in the plane of the OSO-6 rotating wheel. The sun satellite line is defined by the OSO-6 pointed section, which is always within ±3 degrees of the wheel plane, or conversely the wheel plane is always within ±3 degrees of the sun-satellite line. Sun sensors located around the wheel determine when a reference axis in the wheel crosses the sun and the instrument logic establishes the elongation angle of each observation with respect to the sun-satellite line. The satellite had different roll orientations around the sun-satellite line throughout its history, varying between 45 and 90 degrees to the ecliptic. Thus the ±15 degree "cone" of good observations around the anti-sun direction includes data primarily at high inclinations to the ecliptic.

In OSO-6 the roll attitude of the wheel plane was determined by spacecraft magnetometer sensors. In the early data processing the instrument optical axis attitude was calculated for all orbits from 584 to 7600. In the more recent processing we have relied on crossings of known stars to determine the roll attitude and thus the sky coordinates.

The accuracy of the sky coordinate data used throughout our analysis efforts is within one degree of true location, or less than one half

the instrument field of view. This has led to positive identification of stars and permits the detailed mapping of the Milky Way regions and accurate correction for the integrated star light background.

1.5 SCATTERED LIGHT

Of great importance in a space experiment is the reduction to a minimum of instrumental scattered light. This is especially true for observations of low-light-level phenomena such as the several components of the light of the "night" sky. If the OSO-6 photometer had been operable during satellite night the minimizing of scattered light would not have been critical; but since the experiment was designed for the measurement of night-sky-level phenomena during satellite daytime -- that is, with the sun in the sky after the satellite had emerged out of the terrestrial shadow -- instrumental scattered light was a prime consideration.

Unfortunately, the photometer was not adequately baffled and scattered sunlight was overwhelming if the sun was within 90 degrees of the line of sight. A significant fraction of the half of the data for which the sun was more than 90 degrees from the line of sight was affected by the sunlit earth. The residue of good observations, concentrated in a cap centered on the counter-sun direction, a region that surrounds the natural phenomen called the counter-glow (in English) or the gegenschein (in German). In the course of a year the counter-sun line of sight traverses the entire ecliptic and a glance at a sideral map or globe shows that the ecliptic cuts across the Milky Way twice, once near the direction toward the galactic center and six months later (or earlier) near the anti-galactic center direction.

In order to make a critical assessment of the role of instrumental scattered light in our observations with particular reference to Milky Way traverses, we have made a study of the problem. What we need ideally is a light source that exactly fills the photometer field (2 degrees in diameter), which we can then progressively move away from the line of sight, making careful measurements of the

the photometric response as a function of angular departures from the optical axis. Fortunately, nature provides a reasonable standard in the moon, which at and near full phase traverses the counter-sun domain, moving about 15 degrees per day, or 13/15 degrees = 0.87° per orbit. The center of the moon crosses the 2-degree field in 2/0.87 ≈ 2.3 orbits (for a central passage). In ±1 day around full moon we can get a series of readings of ±13 degrees in extent, which turns out to be sufficient for our purpose.

In Table 1-2 we show a typical set of scattering data, allowance having been made for the fact that the moon, with its ½-degree angular diameter fills only 1/16 of the photometer field (this is necessary since we are concerned with surface photometry problems in which we wish to learn the degree of contamination from scattered light from extended light sources similar to the one which is directly in the field). A plot of the scattering coefficients using a logarithmic ordinate is shown in Figure 1-6.

We have used these numerical coefficients to determine the total scattered light for the three colors under a number of conditions which simulate natural circumstances, with the results shown in Table 1-3.

The differential effect on color index determinations in a simulated Milky Way traverse is shown in Figure 1-7. The assumed traverse includes the following sequence: 1) uniform sky; 2) osculation; 3) immersion; 4) on a bright Milky Way ridge; and 5) immersion, osculation, uniform sky. The color index subject to the smallest differential is b-r. Errors of up to about 0.04 in the index are indicated in the sense that the central Milky Way index would have a spurious differential of about 0.04 with reference to the same index outside the Milky Way. In a current study of the color of the Milky Way, we have found b-r differential about five times the indicated spurious effect.

1.6 ABSOLUTE CALIBRATION

The basic problem of space-photometer calibration is similar to that

Table 1-2

FRACTIONAL SCATTERED LIGHT VERSUS ANGLE FROM LINE OF SIGHT

Angle from Line of Sight (deg)	Fractional Scattered Light		
	4000Å	5000Å	6100Å
1.5	0.011475	0.016250	0.008188
2.5	0.005938	0.008688	0.003969
3.5	0.003094	0.004438	0.009062
4.5	0.001594	0.002288	0.000931
5.5	0.000812	0.001188	0.000525
6.5	0.000425	0.000612	0.000212
7.5	0.000219	0.000312	0.000010
8.5	0.000112	0.000162	0.000005

Table 1-3

TOTAL SCATTERING FOR VARIOUS SKY CONDITIONS

Case	Description	Total Scattering (%)		
		4000Å	5000Å	6100Å
1	Uniform sky in all directions	12.1	17.5	7.8
2	Field osculates MW	12.8	18.0	8.2
3	Photometer immersed in a MW gradient	9.7	13.7	6.1
4	Photometer centered on a bright MW "ridge"	8.7	12.1	5.5
5	Photometer centered on a dark MW rift	11.2	16.1	7.2

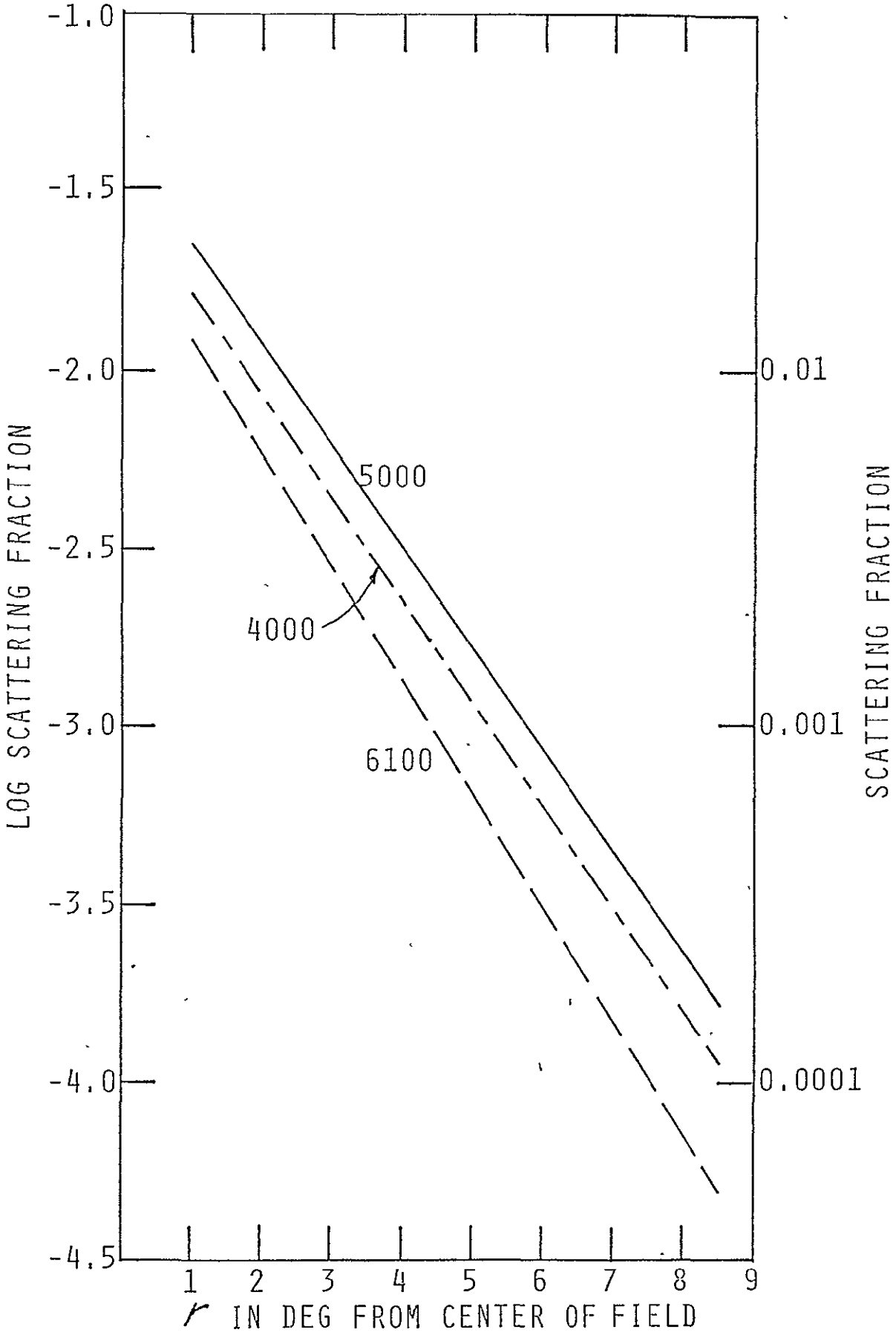


Figure 1-6 SCATTERED LIGHT COEFFICIENTS

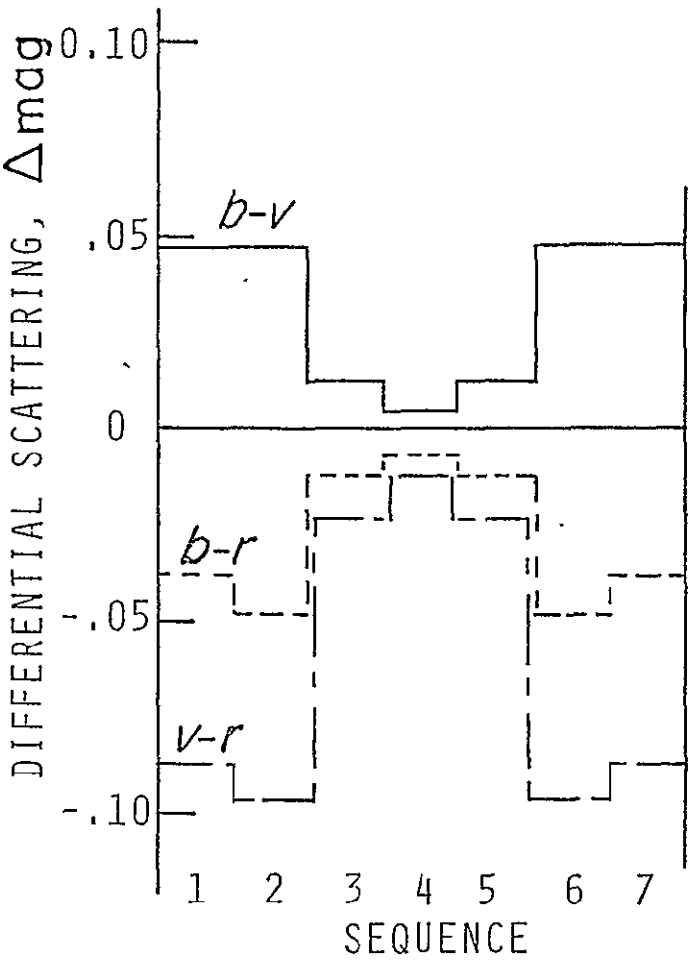


Figure 1-7 DIFFERENTIAL SCATTERING EFFECT ON MILKY WAY COLOR INDEX DETERMINATION

of ground-based instruments, if the observed light is a "surface". We have a paradox -- the measurement of radiation in the laboratory is sufficiently accurate to permit physicists to achieve remarkable success, for example in the determination of black-body radiation curves for various absolute temperatures with wavelengths as the argument: and astronomers using photoelectric techniques often achieve a precision of 0.01 stellar magnitude (about 0.1 percent). The paradox is that several decades of observations both on the ground and in space of the components of the Light of the Night Sky (airglow, zodiacal light, integrated starlight, diffuse galactic light) have been plauged with uncertainties that make it diffucult to make exact intercomparisons of the results of independent observers. During the International Geophysical Year one of us (FER) made a round-the-world trip with a standard light (surface of a fluorescent material impregnated with carbon 14) and a portable photometer to make on-the-sopt intercalibration of airglow photometers in Russia, France, Japan, and the United States. He found that the highly competent individual investigators were subject to calibration differences (errors?) of the order of 10 percent. This is in marked contrast with the 0.1 percent precison cited above for astronomical photoelectric observers working with large telescopes.

It is our considered opinion, after several decades of preoccupation with the problem, that the basic difficulties are of a double and interrelated nature. First, most of the observational material is based on telescopes with relatively small collecting apertures, which therefore require a large field to assure flux adequate to give a reasonable photoelectric response. Second, the use of point sources (stars) as standard light sources to determine calibration coefficients is not uniformly sensitive over the surface.

In the case of a large research telescope such as the astronomers use, the field size is orders of magnitude smaller than is customary in surface photometry. For example, in a current study of the diffuse galactic light, FER used a field aperture of 26 arcsec. Contrast this with the 2-degree (7200 arcsec) field aperture in the OSO-6 photometer. One ploy that has become common in surface photometry using large fields is to include in the optical path a field lens (Fabry optics) which ideally spreads the light from a point surface over a constant area of

the cathode. The OSO-6 photometer was part of a telescope system with the following characteristics.

Aperture	60 mm (2.4 in.)
Field Aperture	2 degrees
Field Lens	Fabry Type
Field Area	3.1416 sq. degrees

The observing ritual is pertinent and is here reported.

1. The OSO-6 was locked onto the sun with good accuracy.
2. The elongations were determined with respect to the sun.
3. Approximately 15 orbits were completed each calendar day.

The sun's movement along the ecliptic, which is due to the earth's revolution around the sun, is about 1 degree per day -- actually $360/3625.25 = 0.986°$ per day. A star that is included centrally in one of the programmed elongations will cross the field of the photometer in about 2 days or 30 orbits. In the calibration of the OSO-photometer, we have used star crossings along with independent comparisons of space readings and ground measurements of surface phenomena. These will be outlined seriatim.

1.6.1 Calibrations Using Stars

Suppose a star of known apparent visual magnitude, m_v, is observed to have a reading of r above the sky background. A more-or-less standard unit in surface photometry is S_{10}Vis, the number of stars of apparent visual magnitude 10 in 1 square degree, which corresponds to the flux from the actual surface. The particular star of magnitude m_v corresponds to n 10th-magnitude stars

$$n = 10 \exp [0.4 (10 - m_v)]$$

For example, the star α Virginis (Spica) is of $m_v = 1.2$. For this star

$$n = 10^{3.52} = 3,311$$

In the OSO-6 photometer with its 3.1416 square degrees, the actual sky reading will be π times higher than it would have been with a 1-square-degree field; hence the calibration factor, k, in this case is

$$k = \frac{3,311}{3.1416\ r} = \frac{1,054}{r}$$

We have found that, even with the Fabry optics, we do not get consistently flat-top star crossings and so have used extensively an auxiliary method of calibration that employs our ground-based knowledge of the Milky Way and the zodiacal light.

1.6.2 Calibrations Using Ground-Based Milky Way and Zodiacal Light Information

One important advantage in space calibrations is that the satellite is usually above most or all of the terrestrial airglow unless tangential observations toward the earth's limb are made. In ground observations, the airglow is either a contaminant in astronomical observations or, if the investigator is an upper-atmosphere researcher, it becomes the primary interest and the astronomical features of the LONS are the contaminants.

In the OSO-6 experiment, the sky is covered systematically and we have, during this project, concentrated on a counter-sun cap which includes the general gegenschein region but also crosses the Milky Way, once per year near the direction toward the galactic center and once in the direction away from the galactic center. Thus it is possible to compare ground-based absolute measurements of the zodiacal light and Milky Way with the OSO-6 readings to obtain calibration curves and constants. The sources we have used are:

1. Roach and Megill "The Integrated Starlight Over the Sky", NBS Technical Note No. 106, 1961; see also Astrophysical Journal, 133, 228, 1961.
2. Smith, Roach and Owen, "A Photometric Map of the Milky Way", Battelle Northwest Report BNWL-1419, UC-2, 1970.
3. Roach, F.E., "A Photometric Model of the Zodiacal Light", The Astronomical Journal, 77, 887, 1972.

The essence of the method is illustrated in Figures 1-8 and 1-9 of this section. Figure 1-8 shows data for a crossing of the Milky Way at an elongation of -170° during the summer of 1971. The ordinate is the value of the summation of starlight, diffuse galactic light (from Smith, Roach and Owen), and zodiacal light (from Roach 1972). The abscissa is the reading, L, from OSO-6. In this case the direct space readings were corrected for satellite temperature before applying a linearizing factor to the original readings which were the result of the quasi-logarithmic response of the OSO-6 amplifier. An orthogonal least squares solution gives the following calibration equation:

$$S_{10}\text{Vis} = 1.904\ L - 88$$

which is shown as the straight line on the plot.

In Figure 1-9 we have applied the calibration equation to the invidividual space observations and show them plotted as the line in which a double abscissa gives either the day in the year or the galactic latitude of the observations. For comparison we display the individual ground observations as unconnected dots. Of course, since the ensemble of space data was calibrated via the ground observations, the general agreement of the two has been forced, but the general quality of the fit is discernible in Figure 1-9.

1.6.3 Integrated Calibration

In the previous section we have shown a calibration based on one set of observations of a crossing of the central Milky Way region. We have extended this analysis to include other sets of crossings as well as several star crossings. This has resulted in a final calibration shown in Figure 1-10, which has a different slope and intercept from that of Figure 1-8. This is due to the heavier influence of the star crossings in the analysis, as well as using the gain relationship that yields proper color indices (which results in a lower linear count for a given telemetry count).

Using the Figure 1-10 calibration we have converted to the history data of Figure 1-11, which is the total brightness observed. The probable

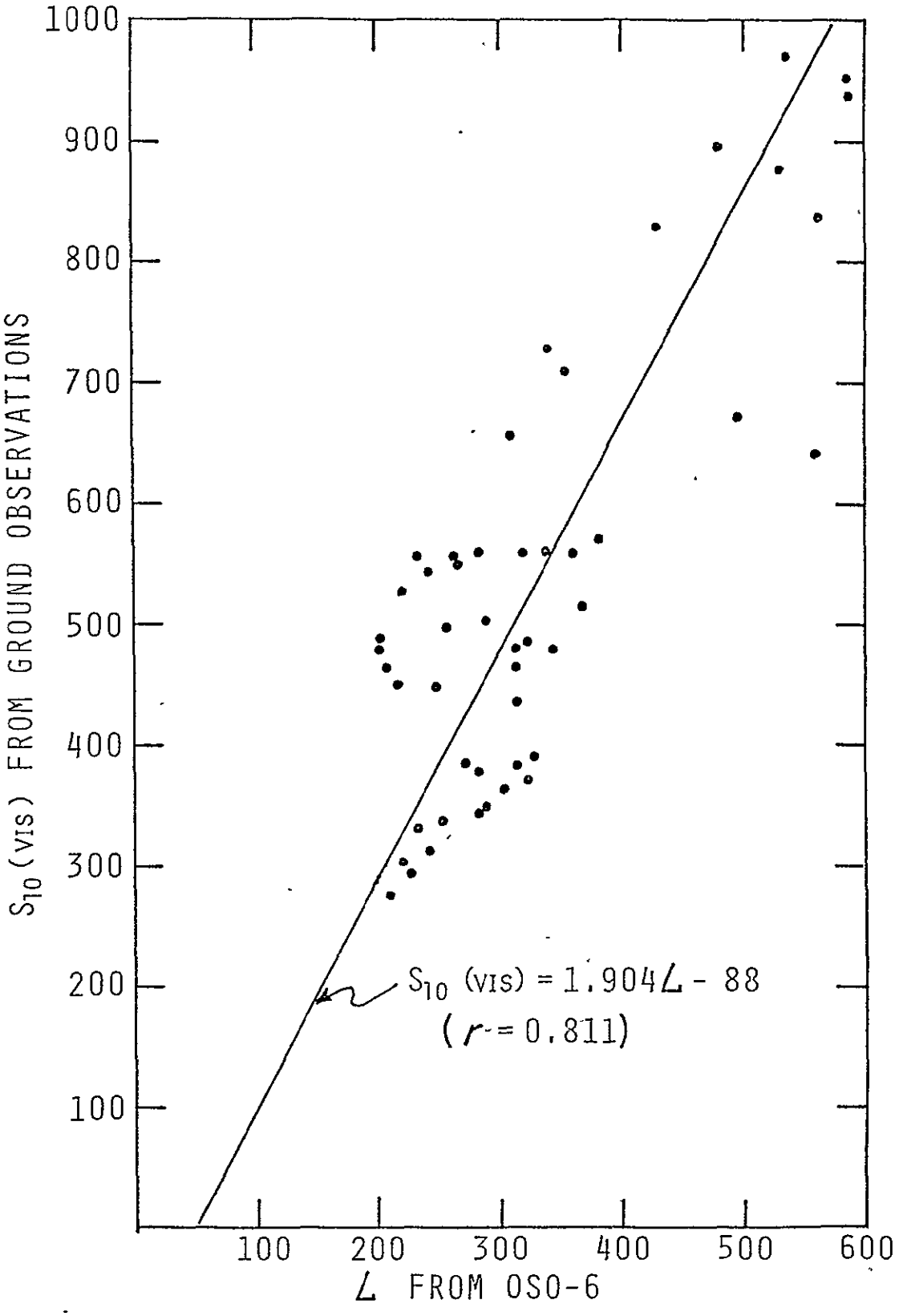


Figure 1-8 ABSOLUTE CALIBRATION IN S_{10} VIS FOR MILKY WAY CROSSING

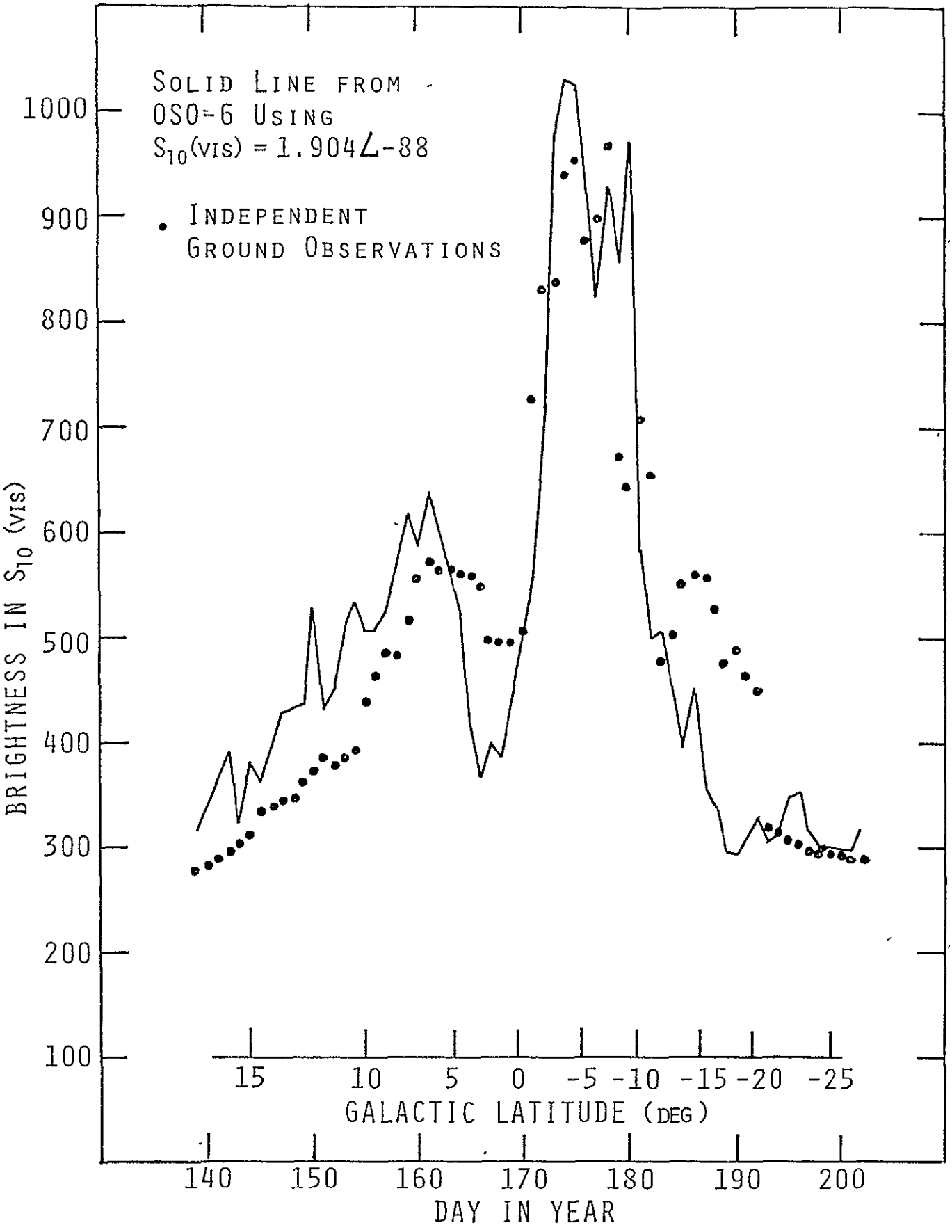


Figure 1-9 COMPARISON OF MILKY WAY CROSSING BRIGHTNESS WITH GROUND OBSERVATIONS

error of the Figure 1-10 calibration is in the order of ±10 percent. This error may be reduced as we add more star crossings to the analysis and remove the scattered light contribution from the Milky Way readings. Note also that the 150 counts residual at zero brightness is a collective term of dark current and radiation effects which weren't previously removed from the data. When the star crossing counts are underdrawn (background removed) and the calibration established the residual counts are zero for zero brightness.

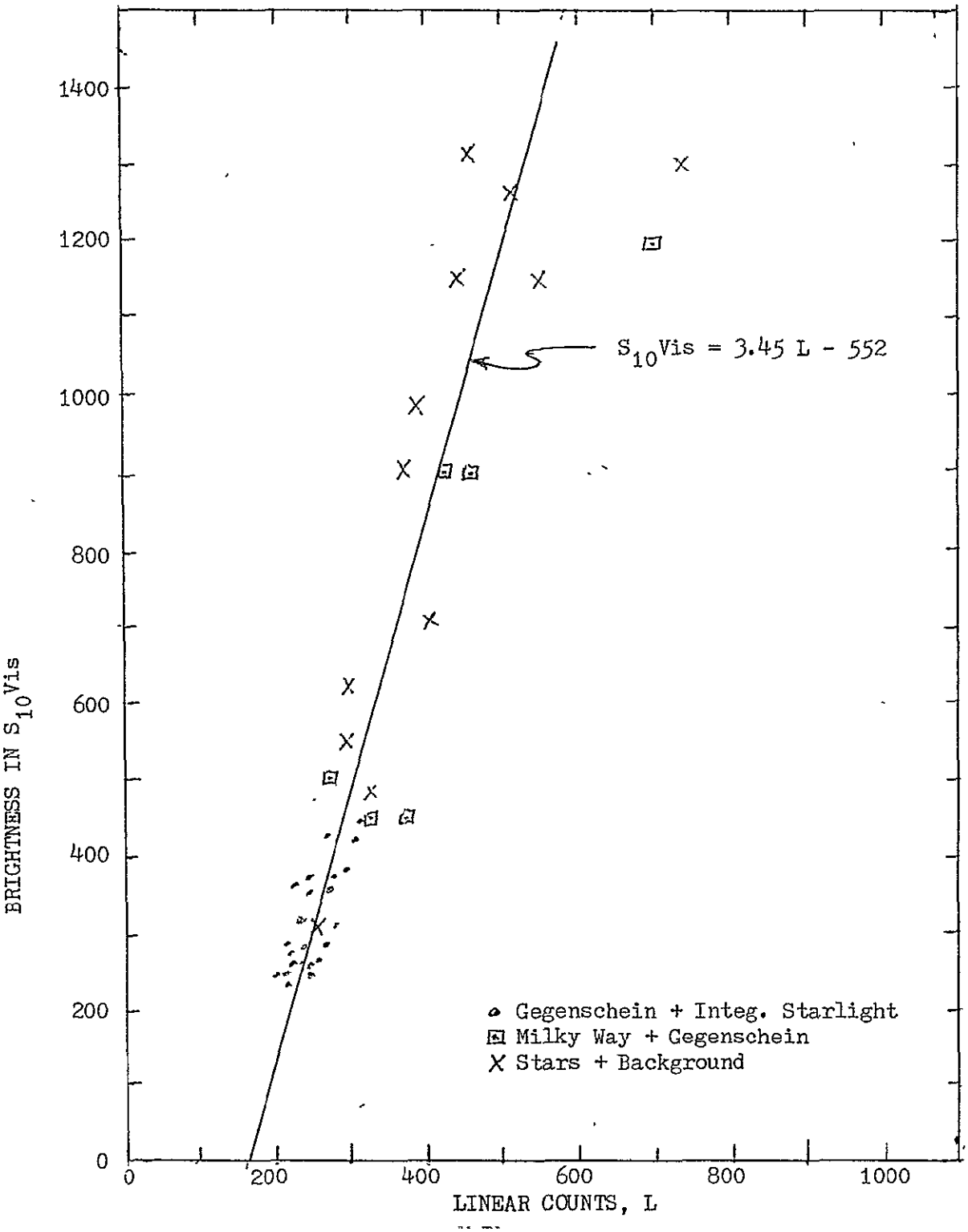


Figure 1-10 ABSOULTE-CALIBRATION IN S_{10} VIS USING MILKY WAY PLUS STAR CROSSINGS

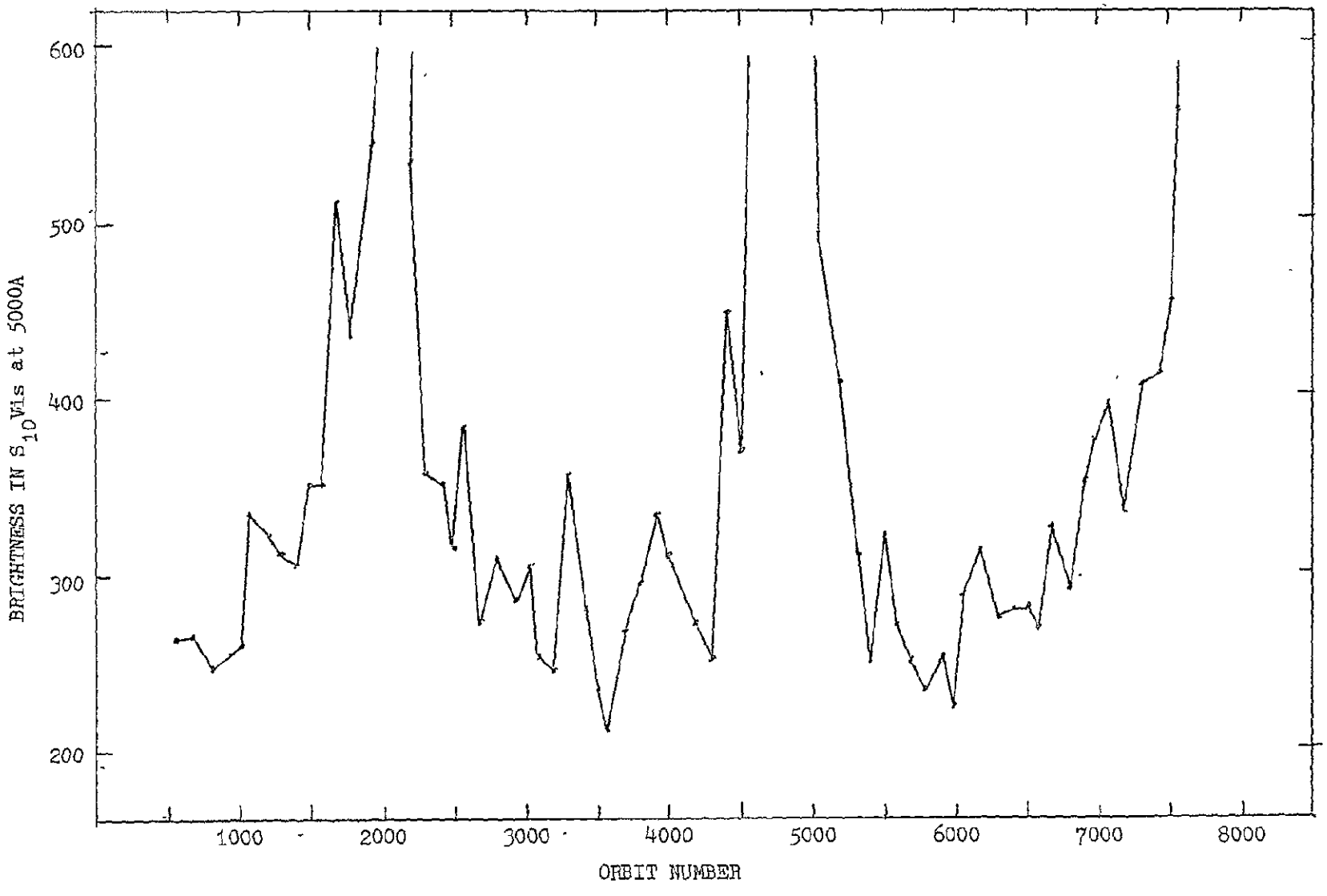


Figure 1-11 DATA HISTORY IN TERMS OF S_{10} VIS

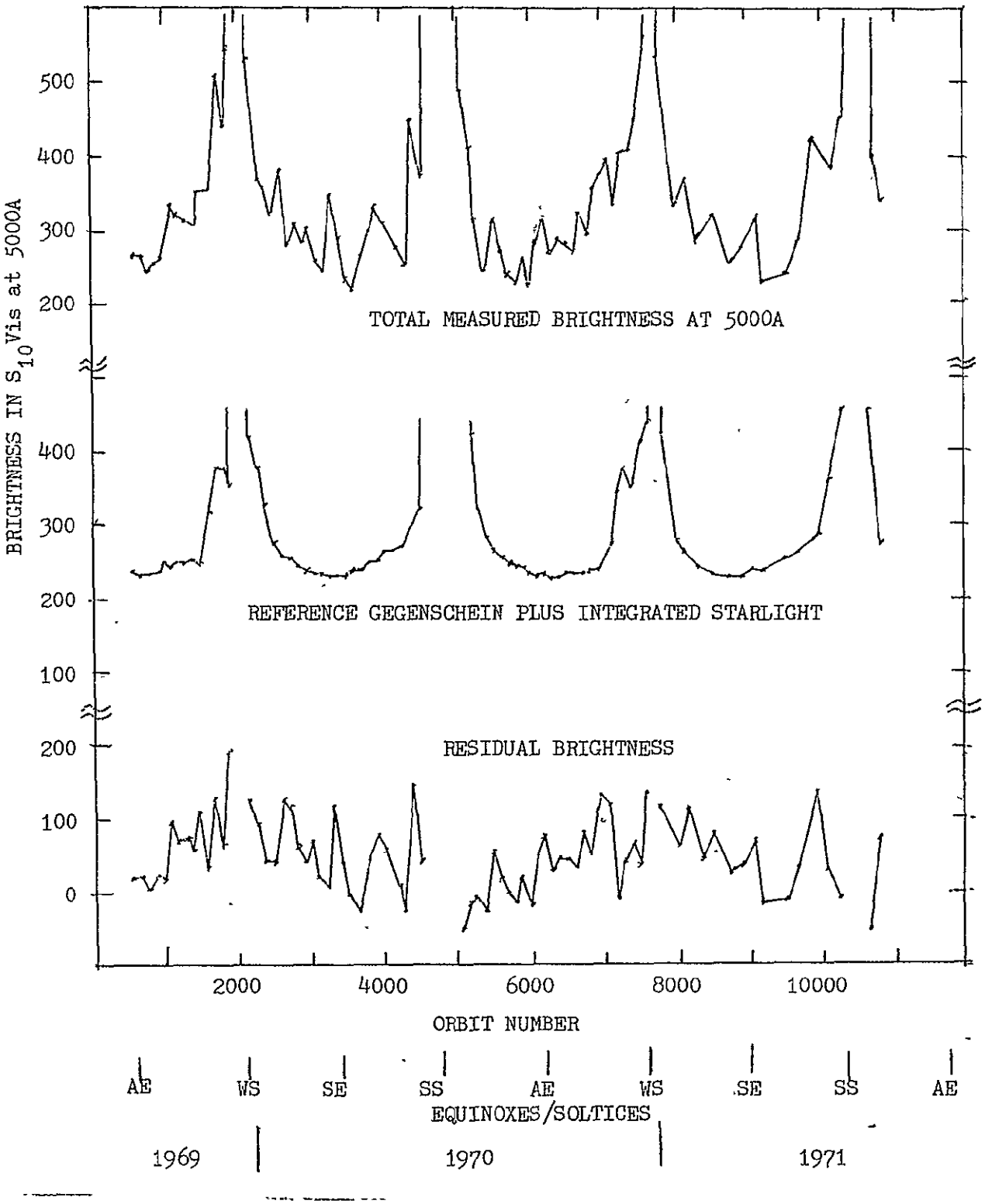
2.0 ZODIACAL LIGHT VARIATION ANALYSIS

Analysis and interpretation of the OSO-6 Zodiacal Light experiment data has been underway since launch. However, the complexities of the necessary instrumental corrections to the data, have limited the analysis to relative effects only, that were independent of the final form of the data. With the major improvement of the data accomplished during this study we have been able to initiate several analyses that have provided significant new information. One of the key areas has been to make use of the long term data baseline of constant sky orientation, to determine any temporal variation in the sky brightness. Secondly, one of us, FER, has included an analysis of the complete 40 year body of ground based data to determine any seasonal variation in the evening/morning ratio of the inner zodiacal light. This section covers these two major analysis efforts.

2.1 LONG TERM GEGENSCHEIN VARIATION

One of the major unique values of this experiment's data is that we have a two year baseline of observations of the sky at a constant solar elongation angle. These 10,500 data points, taken in the anti-sun direction (elongation angle of 180 degrees) cover two complete sweeps around the celestial sphere. This observational history provides repeat coverage of all components of the sky background, namely the gegenschein, integrated starlight, diffuse galactic light and discrete stars brighter than visual magnitude 6.5

Starting with the total sky brightness developed in Section 1.6, Figure 1-11, after applying all of the instrument corrections, we have separated the data into two analysis areas: 1) the fainter domain between Milky Way crossings; and 2) the brighter domain of the Milky Way crossings. In the first domain the dominant contribution to the sky background is the gegenschein. To isolate the long term characteristics of the gegenschein, we have subtracted the other contributions from the total sky brightness. In Figure 2-1 we show three histories: 1) the top history is a repeat of Figure 1-11, the total sky brightness; 2) the middle history is the applicable integrated starlight and diffuse galactic light, taken from the model



For Elongation Angle = 180 Degrees

Figure 2-1 COMPARISON OF SKY BACKGROUND BRIGHTNESS WITH MODEL AND RESULTING RESIDUAL BRIGHTNESS

by Roach and Megill (1961) and Smith, et al (1970) plus a constant value of 205 S_{10}Vis for the gegenschein; and 3) the lower history is the residual brightness after subtracting the middle history from the total sky background history.

It is obvious from this residual history that a long term variation in the sky brightness exists with a one year period. We have interpreted this variation to be in the gegenschein for the following reasons: 1) the measured data have been extensively corrected for known effects. The probable error in the measured data could reduce the magnitude of the variations from 70 S_{10}Vis to 30 S_{10}Vis, but would not change the fact of the yearly variation. Unknown environmental effects on the instrument or inefficient correction of the effects described in Section 1.0 would have a strong 51 day periodicity, which is out of phase with this yearly variation; 2) an error in the model of the integrated starlight plus diffuse galactic light of this magnitude, would leave a residual with a ½ year period, since the Milky Way is crossed twice in the one year traverse of the sky; 3) variations in the night time air glow, which may scatter into the field of view would also have a strong 51 day periodicity as the geocentric latitude of observations moves from north to south; and 4) variations in the dimming of the gegenschein as the field of view includes more or less of the earth's penumbral shadow, would also have a strong 51 day periodicity.

Therefore, we conclude that the yearly residual variation is a factor in the assumption of a constant 205 S_{10}Vis over a year's time. It is significant to note that the peak brightness occurs near the winter solstice and the minimum near the summer solstice. This corresponds to perihelion and apehelion and it can be spectulated that the gegenschein brightness variation is simply due to the variation in solar flux in the vicinity of 1 au. However, the magnitude of the variation is much greater than the 2% change in solar flux and would require a significant increase in the particle density in the interplanetary medium outward from 1 au.

This analysis is for the data at 180 degrees solar elongation. The companion data at ±175, ±170, ±165 degrees solor elongation have been inspected qualitatively and a similar variation is observed.

A detailed quantitative analysis is in order, to determine whether any asymetries exist in the variations as you move off the anti-sun direction. However, this analysis will have to be the subject of future studies.

2.2 EVENING/MORNING ZODIACAL LIGHT RATIOS

The zodiacal light has been extensively observed from the ground over the past 40 years, during which one of us, FER, has been deeply involved in these measurements. During this study we have analyzed this large body of data for variation as a function of geocentric longitude of the observation. Since all ground based data are obtained just before sunrise or just after sunset, the ratio of such observations covers a uniquely different geocentric longitude and thus a different season. By normalizing the body of ground based data to a common model, differences in calibration have been eliminated and a seasonal variation in the evening/morning ratio of the inner zodiacal light (<1 au) has been observed. A draft paper of this result is given in Appendix A.

During this study considerable effort has been made to correlate this result with other ground based data that measures this ratio on a series of nights throughout the year. This large body of data is being processed at SUNY by Misconi and Weinberg, and to date only two ratios have been processed; one confirming the FER result and one ambiguous result. Further comparisons will be made in the future.

3.0 INTEGRATED STARLIGHT AND DIFFUSE GALACTIC LIGHT

The second major analysis of the sky background data we have performed during this study, is of the brighter regions around the crossings of the Milky Way. Once per year the instrument field of view crosses the center and the anti-center regions. These bright regions are a combination of integrated starlight and diffuse galactic light and provide a detail body of data on the color excess of these regions. To date we have concentrated on analysis based on the color excess determined by the b-r index defined in Section 1.3. This index is not appreciable affected by differential scattering in the two wavelength bands. An analysis of interstellar dust based on this index is presented in Appendix B.

Numerical integration techniques have been developed to correct the differential scattering between the 4000, 6100 and 5000 Å data. This will enable us to obtain good color indices involving the 5000 Å data, and thus obtain the color excess for the b-v and v-r indices.

4.0 EARTH/MOON LIBRATION REGION OBSERVATIONS

This experiment has also yielded significant results of another faint region in the sky; the backscatter from the Earth/Moon libration regions. Previous to this study one of us (JRR) has performed extensive analysis of the data from this part of the sky and has shown an increase in the sky background in the direction of the L4 and L5 Earth/Moon libration regions [1]. This enhanced background has been attributed to a backscatter from dust concentrations captured in the libration regions. It has also been shown that this backscatter tends to have a blue signature[2], based on preliminary analysis of the three colors available.

One of the secondary goals of this study was to perform a more rigorous computer analysis of the complete 2½ year history or 29 lunations. The previous analysis was based on 13 lunations and during this study data were obtained for an additional 7 lunations. These new data were qualitatively inspected for a major signature, such as observed for one lunation in the earlier data. To date no such major signature has been observed for the lunations in the new data. The previous hand numerical integration techniques were not applied to the new data, but a computer algorithm was developed and can be applied in future studies with these data, to improve the statistics of the libration backscatter signature.

(1) Roach, J. R., (1975), "Counterglow From the Earth/Moon Libration Points", Planet Space Sci., Vol. 23, pp 173-181.

(2) Roach, J. R., (1975), "The Three Color Characteristics of the Earth/Moon Libration Clouds", IAU Collogium, No. 31, pp 68-72

5.0 DATA PROCESSING

One of the major efforts of this study has been the processing of considerable new orbital data for this experiment. The experiment produced approximately 13,600 orbits of useful data, before the OSO-6 was turned off. These data were supplied by NASA in the form of computer compatible tapes which have been maintained in our tape library throughout this study. Prior to this study approximately 7,300 of these orbits were processed. During this study we have processed an additional 3,200 orbits, to give us a total data base of 10,500 orbits, or about two years of sky coverage. The various processing performed with these data are defined in the following sections. To obtain this additional data base has required approximately 400 hours of operation on the Measurements Analysis Corporation computer facility.

5.1 NEW ORBIT PROCESSING

The processing of the 3,200 new orbits required a multiple step sequence of computer operations. This sequence is defined by the flow diagram given in Appendix C. This complete sequence was programmed, checked out and put into operation during this study. The raw data tapes provided by NASA were generated in the 1970/1971 time frame and were difficult to process on our new generation equipment. Special programming was required to recover the raw data and we successfully recovered over 90 percent of the data tried.

The processing performed prior to this study used algorithms based on our preliminary analysis of the instrument operational characteristics. During this study the iterative analysis of both the old and new data lead to dramatically improved algorithms. These were applied to the 3,200 new orbits and the fourth generation of final linear data was produced. Midway in the study another major improvement in the alogrithm was defined and we re-processed the 3,200 orbits into a fifth generation of final linear data. All of these data are in the form of computer compatible tapes and printouts of the major parameters. The output tapes are maintained in our library and three sets of the printouts were made. The printout format is shown in Table 5-1. Additionally, the final data can be provided in paper tape from for use on

Table 5-1

DATA PROCESSING PRINT FORMAT

ORBIT	DOY	TOD	E40	E50	E51	B-V	B-R	V-R	TB	TW	TR	TAVE	MD	TC
[illegible]	123	15 517	57	170	68	0 196	1 206	1 012	8339	5316	3259	5638	+	23
[illegible]	123	17 60?	5?	173	71	0 134	1 199	1 035	8623	5334	3136	5698	+	25
[illegible]	123	18 167	34	181	78	0 313	1 404	1 068	7361	4941	2826	5050	+	27
[illegible]	123	21 85?	44	111	56	0 009	1 257	1 266	1?444	5214	1393	5634	+	22
[illegible]	123	23 57?	55	166	69	0 194	1 235	1 041	8354	5256	3102	5571	+	27
[illegible]	124	2? ???	57	107	56	-0 323	1 161	1 484	17101	5416	-1497	6340	+	27
[illegible]	124	2? 31?	59	165	72	0 121	1 115	1 108	7036	5272	2397	5668	+	27
[illegible]	124	5 717	48	139	55	0 164	1 148	0 984	8623	5445	3298	5822	+	27
[illegible]	124	1 58?	56	167	71	0 532	1 721	1 062	7541	4443	2947	4311	+	26
[illegible]	124	6 26?	68	180	84	0 755	1 224	1 167	7715	5282	2260	5752	-	25
[illegible]	124	7 ???	66	185	75	0 116	1 134	1 019	7086	5476	3223	5929	+	25
[illegible]	124	10 ???	58	175	75	0 104	1 190	1 086	9208	5353	2836	5799	+	25
[illegible]	124	11 90?	68	179	53	0 046	0 727	0 681	9815	6631	4545	6997	-	25
[illegible]	124	12 501	71	196	83	0 045	1 177	1 132	9826	5381	2532	5912	+	25
[illegible]	124	13 167	47	186	80	0 115	1 195	1 079	9090	5343	2860	5771	+	24
[illegible]	124	15 459	36	179	75	0 730	1 750	1 051	5220	4346	2044	4203	+	25
[illegible]	124	19 782	0	0	0	9 999	9 999	9 999	0	0	0	0	+	27
[illegible]	124	21 533	49	179	75	0 417	1 520	1 104	6714	4747	2726	4729	+	25
[illegible]	124	23 2??	36	188	81	0 797	1 881	1 085	5028	4216	2843	4029	+	4242
[illegible]	125	2? 7??	56	156	12	0 366	-0 744	-0 809	9603	17485	41142	22743	+	25
[illegible]	125	28 717	48	156	57	1 286	1 334	1 048	7606	5066	3062	5145	+	25
[illegible]	125	3? ???	72	185	82	-0 030	1 081	1 111	10704	5600	2675	6326	+	25
[illegible]	125	4 ???	74	190	84	-0 006	1 109	1 117	10439	5535	2637	6203	+	23
[illegible]	125	5 ???	76	184	79	-0 041	1 043	1 084	10835	5693	2853	6461	+	25
[illegible]	125	7 617	77	187	82	-0 036	1 069	1 105	10773	5630	2717	6375	-	25
[illegible]	125	? 55?	34	17?	48	-0 189	0 383	0 572	12888	8077	4963	8643	+	25
[illegible]	125	11 ???	53	257	75	1 203	1 145	1 942	9277	5431	3587	5772	+	23
[illegible]	125	12 ???	75	225	103	[illegible]	[illegible]	[illegible]	7732	5580	4062	5752	-	23
[illegible]	125	?? 86?	51	129	55	0 008	1 095	1 086	10253	5566	2828	6216	+	23
[illegible]	125	16 ???	113	106	22	0 343	-0 821	-1 164	7054	13471	71023	32182	+	26
[illegible]	125	19 06?	77	157	127	0 706	1 308	0 602	4710	4765	4836	4771	+	25
[illegible]	125	25 06?	0	0	129	9 999	9 999	9 999	0	0	0	0	+	24
[illegible]	126	28 26?	57	245	73	0 004	0 681	0 680	10299	6789	4550	7213	+	25
[illegible]	126	29 3??	34	[illegible]	31	[illegible]	[illegible]	[illegible]	0	11117	0	3756	+	23
[illegible]	126	30 183	62	233	113	0 571	1 678	1 106	5891	4507	2707	4369	+	23
[illegible]	126	3 ???	126	390	109	0 221	0 846	0 615	8041	6241	4788	6356	+	23
[illegible]	126	6 167	119	275	115	1 131	0 876	0 715	5637	6150	4425	6411	+	23
[illegible]	126	7 26?	132	374	115	0 193	0 850	0 716	8914	6229	4421	5521	+	23

ORIGINAL PAGE IS OF POOR QUALITY

FER's computing equipment. Only test tapes have been made and a complete production of all the data was postponed pending final resolution of the algorithms.

5.2 OLD ORBIT PROCESSING

The 7,300 orbits of data processed prior to this study were available to us in the form of computer tapes and printouts. The data had been linearized using an instrument calibration algorithm that was made obsolete by the analysis of this study. However, the first processing step was still valid and these data were used extensively in our current analysis. The new processing algorithms were set up to accommodate this old data, but no computer processing was performed, pending final resolution of the best conversion algorithm. Instead selected orbits were re-processed by hand to provide the data analyzed in Sections 2 and 3.

5.3 ANALYTICAL PROCESSING

In the process of analyzing the data base of 10,500 orbits we have performed extensive hand calculations and correlation of parameters. These have included averaging much of the data by every 15 orbits to obtain the values for the half angle of the field of view. These data have been plotted to define the history and cross plotted to determine the proper conversion algorithms. Correlation coefficients have been calculated using the FER computer. Numerical integration techniques have been developed to correct for scattered light effects. Many detailed analysis steps have been used to correlate data with orbital geocentric position; solar elongation angle and with look angle in various coordinate systems such as galactic coordinates and Earth/Moon coordinates. The several years of analysis of these experiment data have provided us with a detailed insight into the various operational characteristics of the instrument. Using this insight we have been able to perform the analysis of the instrument performance and produce useful scientific information.

5.4 SOFTWARE/DATA FORMATS/TAPE LIBRARY

The software developed during this study is described in Appendix C. The processing steps to obtain the basic data from the NASA provided raw data involves extensive manipulation of the data to get it in the correct form. The software for this step is written in assembly language for the Measurements Analysis Corporation Interdata 7/16 computer. The other processing steps are all written in Fortran V language for operation on this same computer facility.

The various generations of data and records obtained during interim processing steps are on file. Considerable detailed data are on the tapes that have not been printed, such as the polarization information. These data are readily available if new studies of polarization are initiated. All final output data of the photometric results have been printed in triplicate; two copies are on file at Measurements Analysis Corporation and one copy is on file with FER.

Extensive computer tape libraries are being maintained at Meaurements Analysis Corporation for all of the raw data, interim data, and final output data. The raw data tapes from NASA include the complete 13,600 orbits of experiment data; the complete command history for OSO-6; and the attitude/orbit history for the OSO-6. Interim data tapes have been retained for the first step of converting from raw data to properly formatted instrument data. The final data tapes for the 10,500 orbits processed to date are also on file.

6.0 RECOMMENDATIONS

Our research with the OSO-6 Zodiacal Light Experiment data had produced several exciting new results. These have been made possible because of the useful data from the experiment and our detailed analysis of the instrument operating characteristics over the years since the mission was conducted. Our concentrated effort during this current study has resulted in a high fidelity calibration of the instrument data, as well as preliminary interpretation of the physical phenomena observed. This study has brought us to the point where we are ready to prepare these results for publication. We recommend that the follow-on studies be conducted to ensure that these results are published in the following areas:

(1) Zodiacal Light long term (seasonal) brightness variations

(2) Zodiacal Light short term (non-homogenieties) brightness variations

(3) Milky Way color excess maps

(4) Earth/Moon libration counterglow brightness and color signatures.

In addition to completing the above research we recommend that the remaining 3,000 unprocessed orbits of data be processed, to add important information to the analysis of the short term brighness variations in the Zodiacal Light. These variations may have significance in terms of defining the non-homogenieties in the inter-planetary medium and additional data would improve the analysis.

The all important analysis of the polarization of the Zodiacal Light and Galactic Light has been postponed until the absolute calibration for the experiment was established. With the work of this current study we can now proceed with this analysis, and we recommend that further study effort include this research.

The 10,500 orbits of data we have processed to date are now in a form that could be converted for filing in the NASA Data Bank. That is, we can express the sky background brightness observed at the six useful elongations about the anti-sun direction, in physical units. Therefore,

we recommend that these data be re-written onto computer compatible tapes for the Data Bank; along with submission of the calibration used to obtain the data.

APPENDIX A

ZODIACAL LIGHT - EVENING/MORNING RATIOS

THE ZODIACAL LIGHT SEASONAL VARIATIONS, EVENING-MORNING RATIOS

F. L. ROACH

Measurements Analysis Corporation, Boulder, Colorado

and

Institute for Astronomy, University of Hawaii, U.S.A.

Running page head. Zodiacal Light

Address: 2969 Kalakaua Avenue, 605
Honolulu, Hawaii 96815

THE ZODIACAL LIGHT: SEASONAL VARIATIONS; EVENING-MORNING RATIOS

F. E. Roach

Measurements Analysis Corporation, Boulder, Colorado

and

Institute for Astronomy, University of Hawaii U.S.A.

ABSTRACT

Published studies are combined to investigate the seasonal variation of the zodiacal light. In order to compare observations with uncertain calibrations and different color filters a method is introduced in which the separate observers' results are compared statistically with a single model and after normalization combined into a single ensemble. From the seasonal variation so determined predicted values of the evening to morning brightness ratios are made.

Key words zodiacal light--interplanetary dust

I. Introduction

Temporal variations of a seasonal nature in the brightness of the zodiacal light have been studied by many investigators (see Misconi 1975 for an extended bibliography). Visual observations suffer from the difficulty of "calibrating" the observer's eye over an extended period of time. Photoelectric and photographic observations have an advantage because of the possibility of quantitative calibration procedures.

The literature gives an ambiguous answer to the question of the variability of the zodiacal light either seasonally or during a night. Some authors have reported positively and some negatively. Since the writer was co-author of an early paper (Elvey and Roach 1937) indicating a seasonal variation, he has re-examined the subject with the hope of combining the observations of a number of observers into a composite picture.*

II. Analytical Procedure

As is well known to all zodiacal light analysts, the quantitative evaluation of its absolute brightness when using a photoelectric photometer involves two interrelated factors:

1) the absolute calibration of the photometer, and
2) the allowance for the amount of radiation from other sources contributing to the brightness of the night sky light, chiefly the nightglow and the integrated starlight.

The interrelationship between the two is close. If the absolute calibration is in error then the allowance for the "contaminants" will also be in error and this in turn will produce uncertainties in the ZL brightness. Similarly inaccuracies in the priori

---

*A perusal of the classical work of Jones (1856) leaves the reader with the strong conviction that there are short-time brightness variations (over a few minutes). Because of the extraordinary experience of Jones as a visual observer of the zodiacal light his reports deserve a high credibility rating.

knowledge of the contaminants will affect the estimates of the zodiacal light brightness. The nature of the analysis is such that the uncertainty in the final deduced ZL brightness may be a function of the elongation of the observation from the sun, the brighter portions of the zodiacal light being more sensitive to calibration errors (the contaminants being relatively less important than the ZL) whereas, vice versa, the less bright regions are more affected by uncertainties in the contaminant corrections since they constitute a larger fraction of the whole.

The interrelationship between the two is illustrated in Figure 1 and Table I We show three cases: 1) exact agreement with the model recently introduced by Roach (1972) which hereafter we shall refer to as R_1; 2) a hypothetical case in which an error entirely due to calibration is introduced; and 3) a case in which the calibration error of 2) is compounded by a "subtractive" error corresponding to improper allowance for the contaminants. Orthogonal least squares* solutions are indicated in Figure 1 for the three cases.

They hypothetical cases just examined illustrate one feature: the numerical values of a and b in the equation

$$y = a + b\,x \qquad (1)$$

correspond to subtractive (contaminant) and multiplicative (calibration)

---

*Throughout this paper we use "orthogonal" least squares solutions in which neither of the parameters is considered to be independent. Actually the data in Figure 1 and Table I do not call for a least-squares solution since the quantities have been predetermined analytically.

ORIGINAL PAGE IS
OF POOR QUALITY

differences respectively between the model (R_1 and the several observational sets under study, where x may be the case under study and y is R_1. It is noted that, if the subtractive error is constant throughout a particular investigation which may cover a large part of the ecliptic sky, then the separation of the subtractive and the calibration differentials is definitive, that is the intercept in a least-squares solution corresponds to the "constant" difference in allowing for the contaminants and the slope is then an indication of the disagreement in the two calibrations. We use the word "calibration" here to include the possibility that the two sets of observations may involve different color filters and in that case the slope determined by the use of equation (1) is a measure of the color index.

If the subtraction correction for a particular observer is not constant, for example larger for regions of smaller absolute ZL brightness, such a circumstance could contribute to a pseudo calibration differential. Such might occur for example if portions of the observations infringed on the Milky Way or were differentially subject to the vagaries of the nightglow. If, on the other hand, the contaminant corrections are of a random nature with respect to a particular ensemble of ZL observations then the effect on the final results will be a scatter which will yield low correlation coefficients when compared with another observer's results.

In this study we made such comparisons between the R_1 model and a number of published listings of the brightness of the zodiacal light. Included are some examples of observations in the ecliptic

and others of brightnesses away from the ecliptic. In large part the samples refer to solar elongations less than 90° so the scrutiny of the scattering zodiacal cloud cuts through the inner part of the solar system (see figure 2).

In Table II we display the empirical results of intercomparisons in which y in equation (1) is R_1 brightness and x is the sample brightness. Values of a, b, the correlation coefficient, r, and the number, n, of observations are listed. We note the generally high values of the correlation coefficients in Table II, indicating a striking consistency among the several observers. On the other hand the spread in the values of the intercept a (-222 to 637; median -3) illustrates the great difficulty in correcting for the photometric contaminants. The spread in b is due to either or both of the following: calibration differences or color filter differences.

In Figures 3 and 4 we show sample plots of equation (1) in which the y coordinate is from the R_1 model and the x coordinate is from another observational set. The intercepts, slopes and correlation coefficients based on orthogonal least-squares solutions are indicated.

The fundamental approach of this study is demonstrated in the eight cases chosen for illustration in figures 3 and 4. The slopes, b, vary from 0.750 for the "red" observations of Sparrow and Ney to 2.525 for the "blue" Barbier observations. These extreme values of b are obviously due to the color filters and can be used in determining color indices referring to the particular filters used by

the observers relative to the R_1 "visual" filter. On the other hand the slopes 1.088 and 1.156 for the observations of Dumont and Misconi are basically indications of calibration differences between the observers and R_1.

The small scatter of the individual observational points is obvious from inspection of the plots and is reflected by the correlation coefficients listed in Table II which are all higher than 0.9. This indicates very high agreement in the general ZL patterns as deduced by observers working under diverse conditions and over an extended period of time. The entries of Table II and the examples displayed in Figures 3 and 4 all correspond to average ZL maps and we now proceed to examine cases where many nights of observation over seasonal spans entered into these means.

III. Seasonal Variations

We have referred to the slope, b, as due to differences of calibration or color with respect to a combination of two sets of data of which one set is the fixed model R_1. Now we propose that values of b for observations of a given observer for nights spread out over different seasons correspond to seasonal changes in the absolute brightness of the ZL. Implicit in this interpretation is an assumption that any observer's results will have a constant relationship to R_1 so far as calibration is concerned and that the average value of b is indicative of same. In the analysis to be described we interpret the changes of b with respect to the average as due to temporal brightness variations.

From the data included in Table 2 we have abstracted those observations (marked with an asterisk) for which the observer indicated zodiacal light maps for different times of the year. The data were treated in the following steps

1) the average value of $\underline{b}$ was determined for each combination, R_1 versus the other observer,
2) the data were normalized to make $\underline{b}$ (average equal to unity,
3) the observations were then referred to a particular value of geocentric ecliptic longitude, λ, using the median λ for each case.

The data so collected are given in Table III for five intercomparisons with R_1: Elvey and Roach (1937), Roach et al (1954), Regener (1954), Van de Noord (1970) and Misconi (1975). The values of $\underline{b}$ were ordered according to geocentric ecliptic longitude, then smoothed by running 5's. The corresponding values of $\underline{b}^{-1}$ are given in Table III.

The case of Regener's photographic observations illustrates the method. The entry in Table II is the mean of observations on 33 nights and the plot of Regener's mean data is included in Figure 4. The value of $\underline{b}$ given in Table II (1.664) is based on averaging the brightness entries for the 33 nights and running an orthogonal least-squares solution on same But treating the values of $\underline{b}$ for the original nights gave $\underline{b}$ (average) of 2.070. This value was used to normalize the individual values of $\underline{b}$ which had a range from 1.402 (minimum) to 3.236 (maximum). It is this spread of $\underline{b}$

which has been ordered according to ecliptic longitude along with similarly treated data from the four other investigators mentioned in the previous paragraph.

In Figure 5 the smoothed values of $\underline{b}^{-1}$ from Table 3 are shown in a polar plot. We note structure in the zodiacal light suggesting structure in the zodiacal cloud. Two gross features are apparent, a minimum of brightness between longitudes 40° and 123°, a broad maximum from 180° to 300°. Smaller scale features are minima at about 35°, 175° and 340° and maxima at 15° and 135°. These photometric features suggest that the physical zodiacal cloud responsible for the zodiacal light is not uniformly distributed. It should be noted that the temporal span of the composite data of this analysis extends over about three and a half decades (1934 to 1968) and that all the observations fit into the general pattern as shown in Figure 5, so the tentative conclusion is that the zodiacal cloud is at least quasi-stable.

IV. The Evening-Morning Ratios of Zodiacal Light Brightnesses

It is obvious from inspection of Figure 5 that the evening-morning ratio of ZL brightness will vary throughout the year along with the sun's apparent path along the ecliptic In order to obtain a general impression of the nature of this seasonal change it is convenient to take as a parameter the ratio Z

$$Z = \frac{B\ (\varepsilon + 50°)}{B\ (\varepsilon - 50°)} = \frac{ZL\ (\text{evening})}{ZL\ (\text{morning})}$$

where B is the ZL brightness. A plot of this parameter is shown in Figure 6 with date of the sun's ecliptic longitude as the independent

variable. Figure 6 predicts that E/M >1.0 from June to November and <1.0 in January and from March to June. It will be of interest for future ZL observers to test these predictions. The use of the R_1 model in this analysis is for convenience and does not necessarily imply that the model has any claim on absolute accuracy. The use of any other published ZL brightness distributions would have served equally well since we used the technique of normalizing $\underline{b}$ and hence $\underline{b}^{-1}$ for each combination of observations entering into the seasonal study However the R_1 model is especially convenient in that it includes estimates of ZL brightness over the entire sky and can thus be used for comparison with the observations of others over the sky even to the ecliptic pole

V. Conclusions

The present study leads to some tentative conclusions·

1) The evidence of consistency among ZL observations extending over more than three decades suggests that the ZL dust cloud in the inner solar system is quasi-stable.

2) The brightness of the ZL in the plane of the ecliptic is variable over a two-fold range as a function of geocentric ecliptic longitude. The clear implication is that the zodiacal dust cloud is irregularly distributed around the ecliptic. Such irregular photometric distribution suggests possible irregular concentrations of cometary or ateroidal debris in the ecliptic plane as viewed from Earth.

3) A sensitive test of the validity of the present analysis is the systematic study of the evening-morning ratio of ZL brightness on a seasonal basis. If an observer is meticulous in his observational and analytical procedures he can be assured of constancy of calibration throughout a night as well as uniformity in his corrections for contaminant radiations. Thus the ratios should be more reliable than the absolute values themselves.

Table I

Hypothetical Cases of Zodiacal Light Errors

	1	2	3
ε(deg)	y R_1	x_1 1.5 R_1	x_2 1.5 R_1 + 100
30	2330	3495	3595
40	1185	1777	1877
50	745	1118	1218
60	500	750	850
70	370	555	655
80	290	435	535
90	250	375	475

1) $y = x$
2) $1.5\ y = x$
3) $1.5\ y + 100 = x$

ORIGINAL PAGE IS
OF POOR QUALITY

Table II

Comparison of Published Zodiacal Light Observations

$R_1 = a + b \times$ (see text)

	a	b	r	n	Color	Authors
1	- 16	0.567	0.996	7	Red	Wolstencroft and Rose (1967)
2	20	0.750	0.998	9	Red	Sparrow and Ney (1968)
3	- 2	0.851	1.000	15	Vis	Roach and Smith (1964)
4	101	0.930	0.973	9	Vis	Banos and Koutchniy (1973)
5	1	1.001	1 000	13	Vis	Roach et al. (1954)*
6	637	1.058	0 986	4	Vis	van de Noord (1970)*
7	- 38	1 072	0.999	31	Vis	Weinberg (1963)
8	16	1 088	0.987	47	Vis	Dumont (1965)
9	84	1.156	0.993	54	Vis	Misconi (1975)*
10	83	1 217	0.985	34	Vis	Beggs et al. (1963)
11	2	1.241	0.994	47	Vis	Frey et al. (1974)
12	- 55	1 267	0.977	--	Vis	Smith, Roach, Owen (1965)
13	- 16	1 308	1.000	4	Vis	van de Noord (1970)*
14	- 45	1.309	1.000	--	Vis	Peterson (1961)
15	-517	1.321	0.999	4	5915A	Leinert et al. (1974)
16	412	1.323	1.000	4	4680A	Leinert et al (1974)
17	-356	1.446	1.000	4	4755A	Leinert et al (1974)
18	- 16	1.45	1.000	14	Ph	Elvey and Roach (1937)*
19	93	1.509	0 995	22	Blue	Barbier (1954)
20	157	1.664	0 995	25	Ph	Regener (1954)*
21	20	1.863	0.999	6	Ph	Elsässer (1963)
22	- 21	1.876	0.998	4	Ph	Behr and Siedentopf (1953)
23	- 10	2.074	0.994	77	Blue	Gillett (1966)
24	8	2.162	0.956	10	Blue	Sparrow and Ney (1968)
25	-222	2.250	0.986	7	Blue	Wolstencroft and Rose (1967)
26	- 3	2.282	0.993	26	Blue	Pfleiderer (1975)
27	10	2.46	0 999	5	Blue	Lillie (1972)
28	- 13	2.525	0 963	21	U.V.	Barbier (1954)
29	122	2.595	0.998	6	Ph	Fesenkov (1947)
30	- 19	2.778	0.913	65	Ph	Divari (1952)
31	- 41	3.227	0.984	7	Ph	Hoffmeister (1932)

*The studies marked with an asterisk were used in the seasonal variation study.

ORIGINAL PAGE IS
OF POOR QUALITY

Table III

Tabulation of b^{-1} and λ, smoothed by running 5's

λ	b^{-1}	λ	b^{-1}
5 1	1.109	135.2	1.159
9.1	1.203	142.6	1.122
13.4	1.253	151.4	1.068
16.8	1.234	159.0	0.995
19.2	1.196	165.5	0 955
21 3	1.236	172.0	0.911
23 3	1.172	174.6	0.885
24.9	1.109	175.8	0.971
26.8	1.017	177.6	0.991
28.4	0.916	179.4	1.032
30.4	0.836	183.6	1.114
32.2	0.815	188.8	1.225
33.2	0.853	196.6	1 162
34.0	0.934	205.2	1.219
34.8	1.088	219.6	1.177
35.2	1 073	240.2	1.129
35.8	1.058	240.6	1 152
36.5	0.970	278.4	1 206
37.2	0.973	295.0	1.196
38.2	0.869	306.4	1.215
39.3	0.879	309.4	1.189
40.3	0.879	311 6	1.261
41 9	0 859	313.6	1 295
43.3	0.849	316 4	1.312
46.3	0.831	318.8	1.295
49 6	0.833	320.6	1 321
52.8	0.785	322.4	1.164
56 0	0.766	325 8	1.022
64.8	0.718	328 4	0.963
75.8	0.744	331.4	0.962
86.8	0.719	337.4	0 930
100.6	0.792	344.4	0.946
113.8	0.859	350.8	1 031
122.8	0.935	358.2	1.069
128.9	1.016		

Banos, C , and Koutchmy, S. 1973, Icarus 20, 32

Barbier, D. 1954, International Astrophysical Symposium Report, Liege, pp 55 ff

Beggs, D. W., Blackwell, D E., Dewhirst, D. W and Wolstencroft, R 1963, M N.R.A.S. 127, 319.

Behr, H., and Siedentopf, H 1953, Zs F Aph. 32, 19.

Divari, N. B. 1952, Astronomicheskii Zhurnal 29, 1, 49.

Dumont, R. 1965, Anales D'Astrophys. 28, 255.

Elsasser, H. 1963, Plan. and Sp Science 11, 1015

Elvey, C T., and Roach, F. E 1937, Ap. J 85, 213

Fesenkov, V. G. 1947, Meteoric Matter In Interplanetary Space, Academy of Sciences Press (Russian).

Frey, A., Hoffmann, W., Lemke, D., and Thum, C. 1974, Astron. and Astroph. 36, 447.

Gillett, F. C. 1966, Ph.D Dissertation, Univ. of Minnesota.

Hoffmeister, 1932, Veröff der Univ. Sternw. zu Berlin-Babelsberg, 10, NR. 1.

Jones, George 1856, Observations of the Zodiacal Light, United States Japan Expedition, Volume 3.

Lillie, C. F. 1972, NASA SP-310, pp 95 ff

Leinert, C , Link, H., and Pitz, E. 1974, Astron. and Astrophysics 30, 411.

Misconi, N. Y. 1975, Ph.D Dissertation, State University of N.Y. at Albany.

Peterson, Alan W. 1961, Ap. J 133, 168.

Pfleiderer, J. 1975, Personal Communication.

Regener, V. H. 1954, Final Report, Univ. of New Mexico, Contract AF19 (604) 118.

Roach, F. E., and Smith, L. L. 1964, N.B.S. Tech. Note 214

Roach, F. E., Pettit, H., Tanberg-Hannsen, L., and Davis, D. 1954, Ap. J. 119, 253.

Roach, F. E. 1972, Astron. Jnl. 77, 887.

Smith, L. L., Roach, F. L., and Owen, R. W. 1965, Plan. Sp. Sci. 13, 207

Sparrow, J. G., and Ney, E. P. 1968, Ap. J. 154, 783.

van de Noord, L. L. 1970, Ap. J. 169, 309

Weinberg, J. L. 1963. Ph.D. Dissertation, Univ. of Colorado.

Wolstencroft, R. D., and Rose, L. J. 1967, in The Zodiacal Light and the Interplanetary Medium, NASA SP-150, pp. 49-56

Captions for Figures

Fig. 1 Comparisons of the ZL model R_1 with three cases: (1) exact agreement between R_1 (ordinate) and the hypothetical observer, (2) the calibrations differ by 1.5, and (3) both the calibrations and the contaminant corrections differ (see Table 1 and text.

Fig 2 Illustration of the line of sight of ZL observations for elongations up to 90°.

Fig. 3 Correlation plots of the ZL brightness, R_1 versus four different observers.

Fig. 4 Correlation plots of the ZL brightness, R_1 versus four different observers.

Fig. 5 Polar plot of b^{-1} from Table III.

Fig. 6 Polar plot of L/M (evening-morning brightness ratio of ZL) predicted from results in Table III.

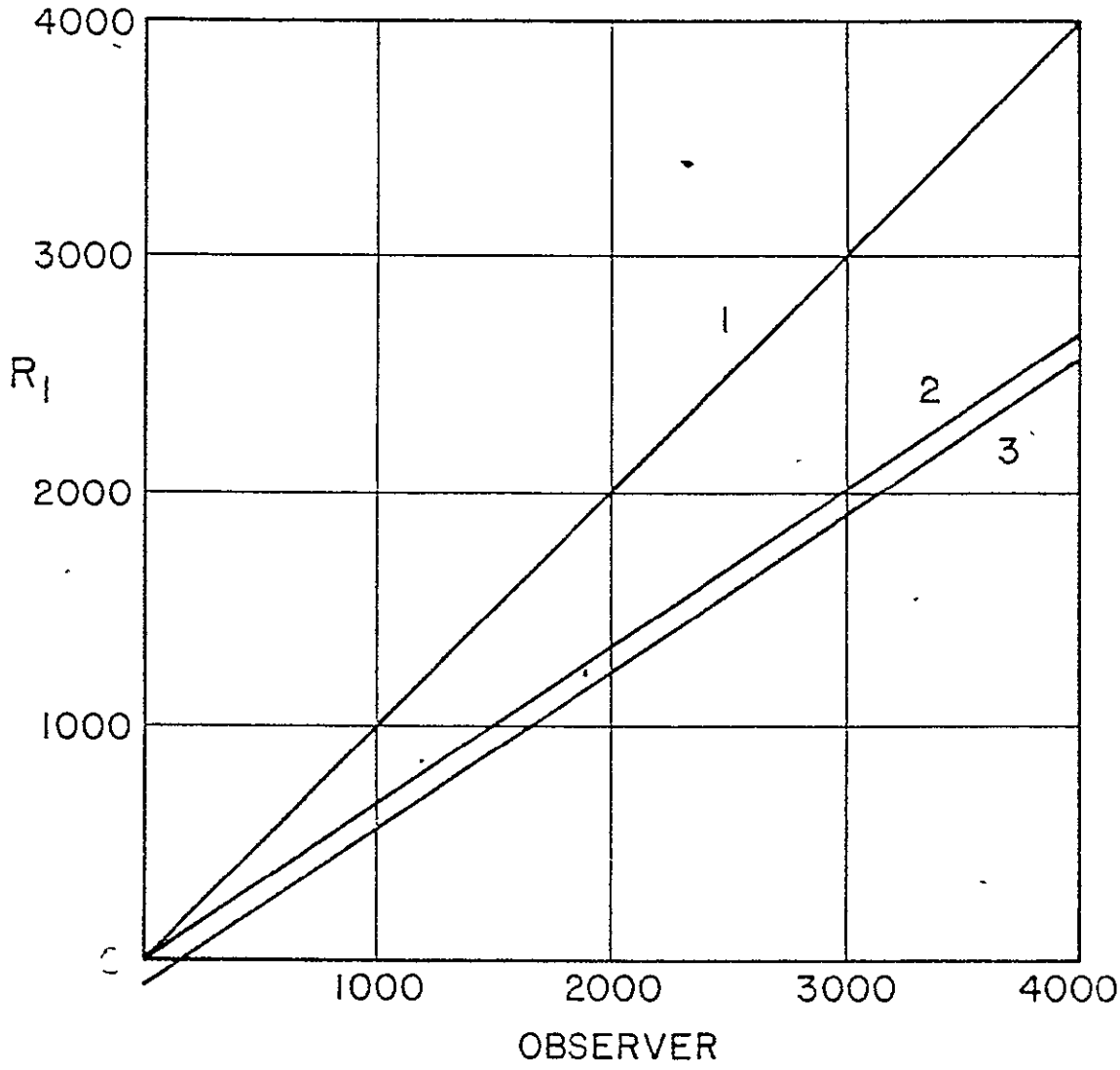


Figure A-1 COMPARISON OF ZODIACAL LIGHT MODEL WITH THREE CASES

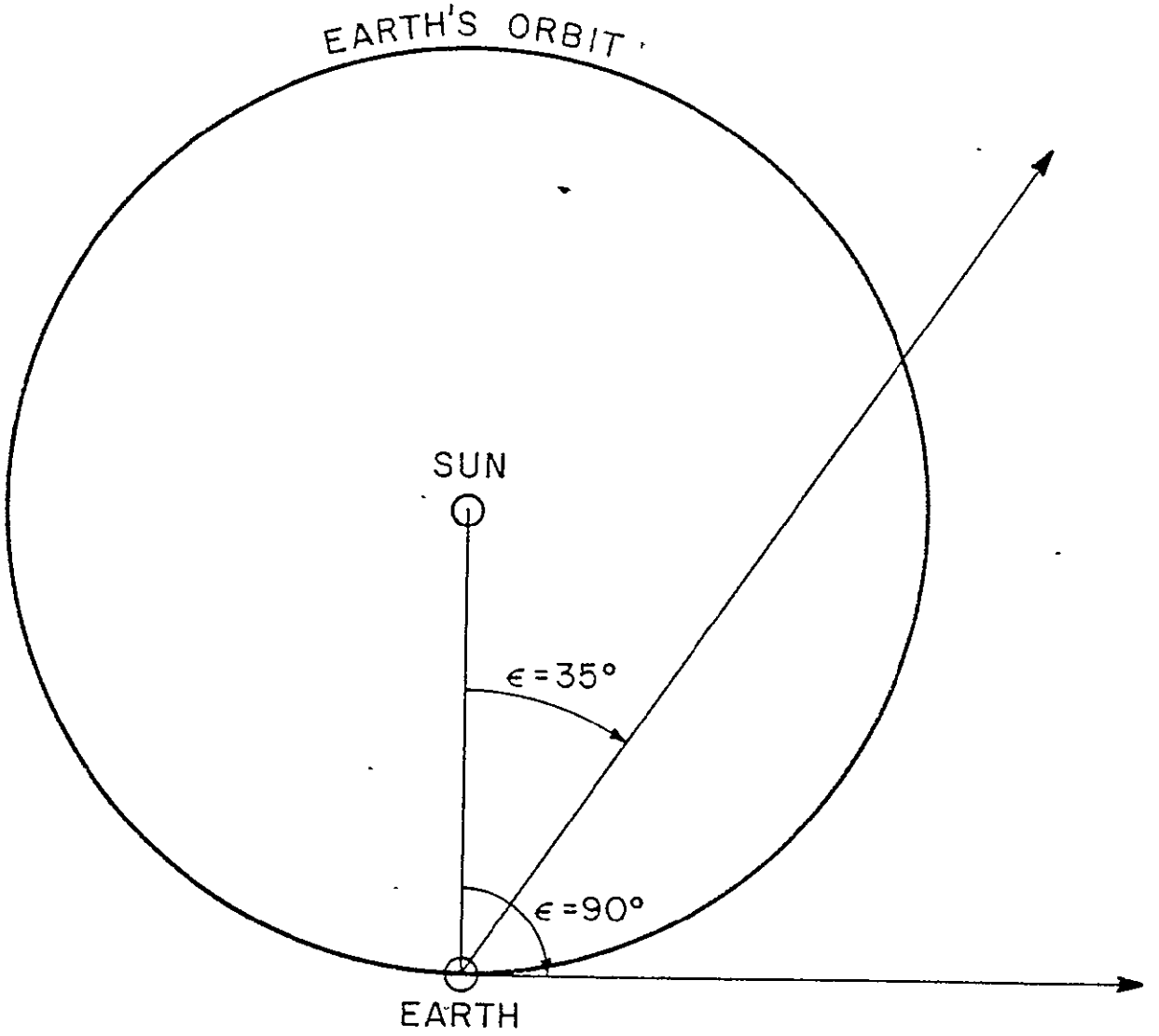


Figure A-2 ILLUSTRATION OF LINE OF SIGHT OF ZODIACAL LIGHT OBSERVATIONS

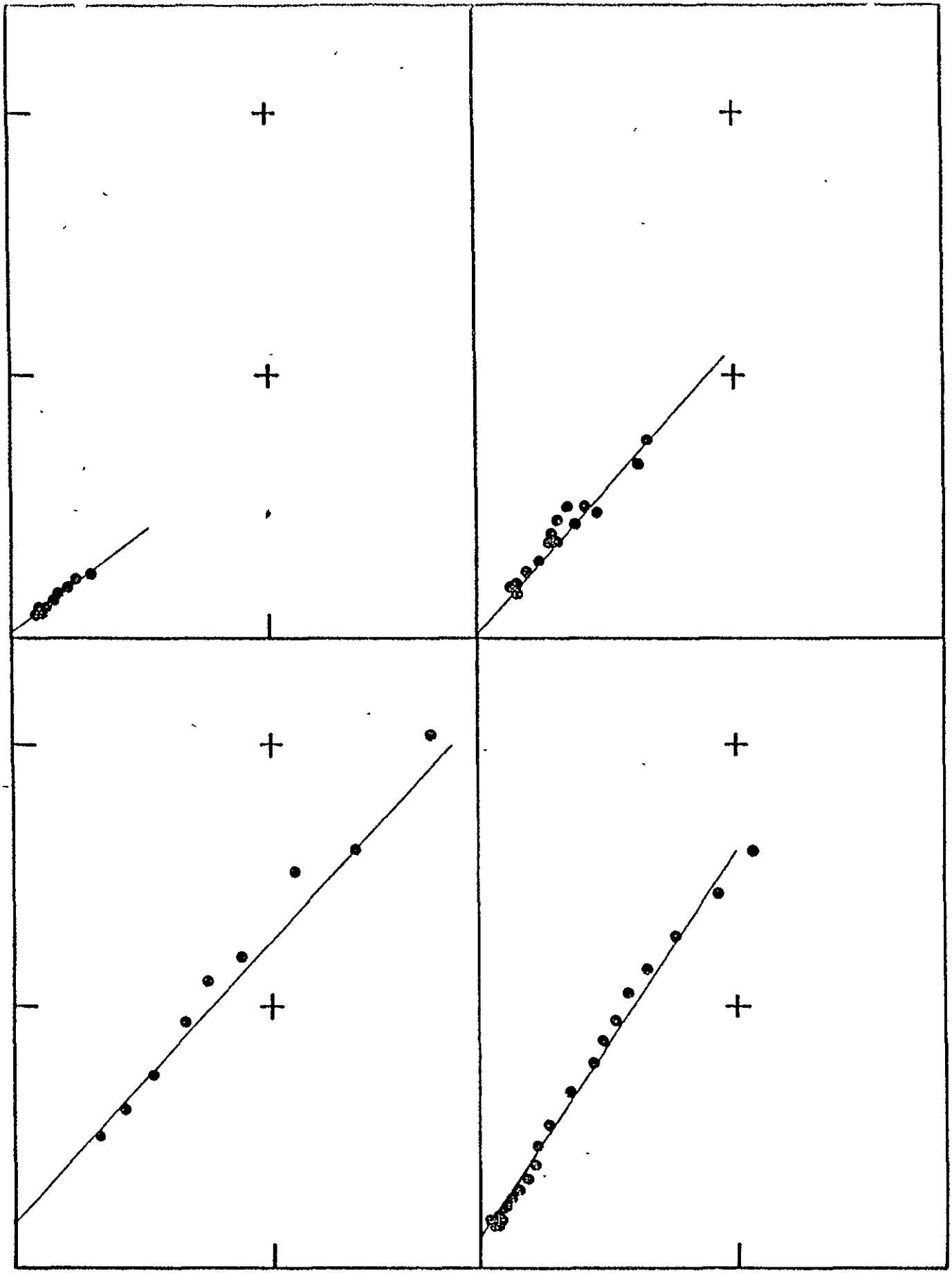


Figure A-3 CORRELATION PLOTS OF THE ZODIACAL LIGHT BRIGHTNESS

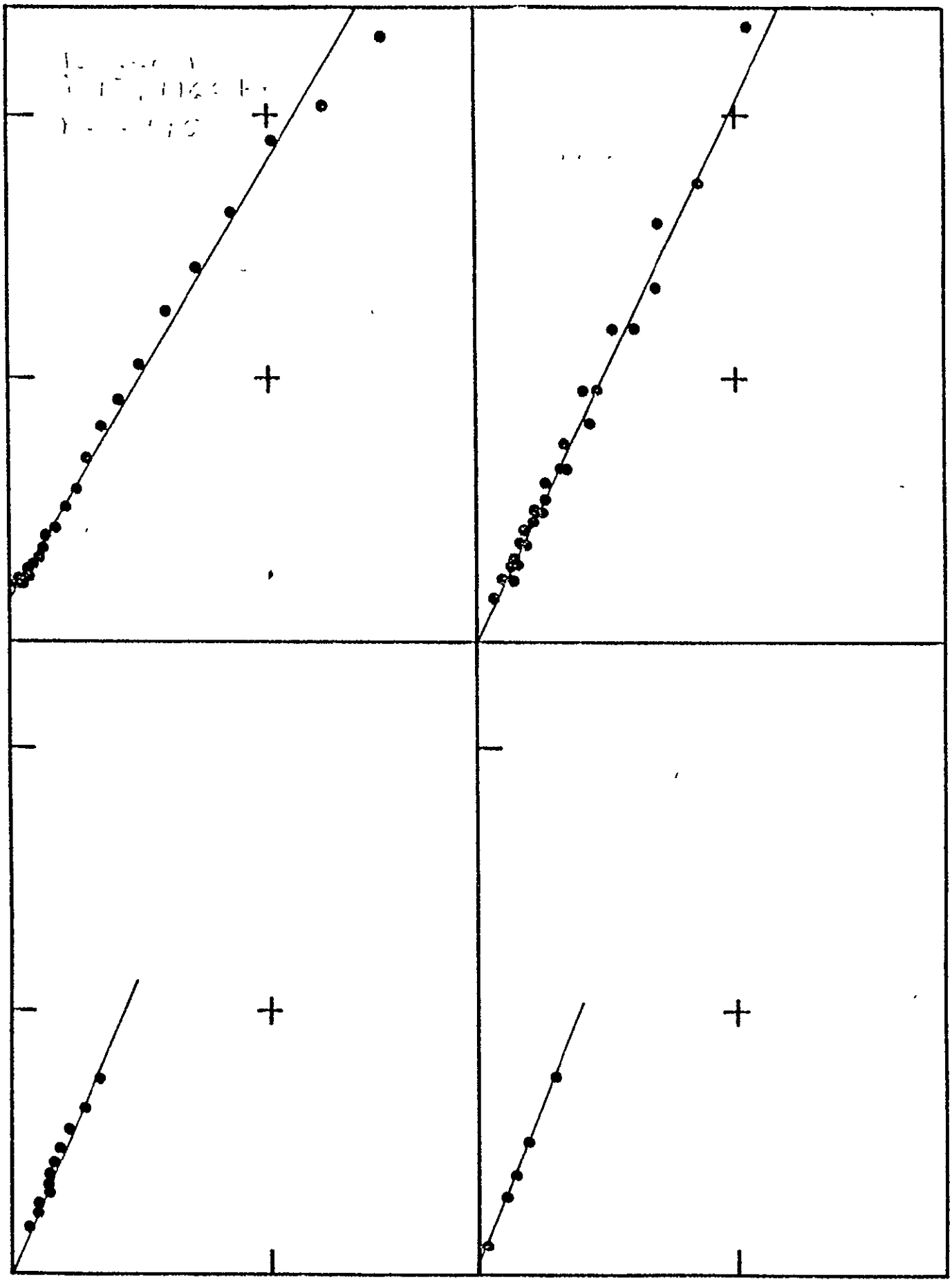


Figure A-4 CORRELATION PLOTS OF THE ZODIACAL LIGHT BRIGHTNESS

ORIGINAL PAGE IS
OF POOR QUALITY

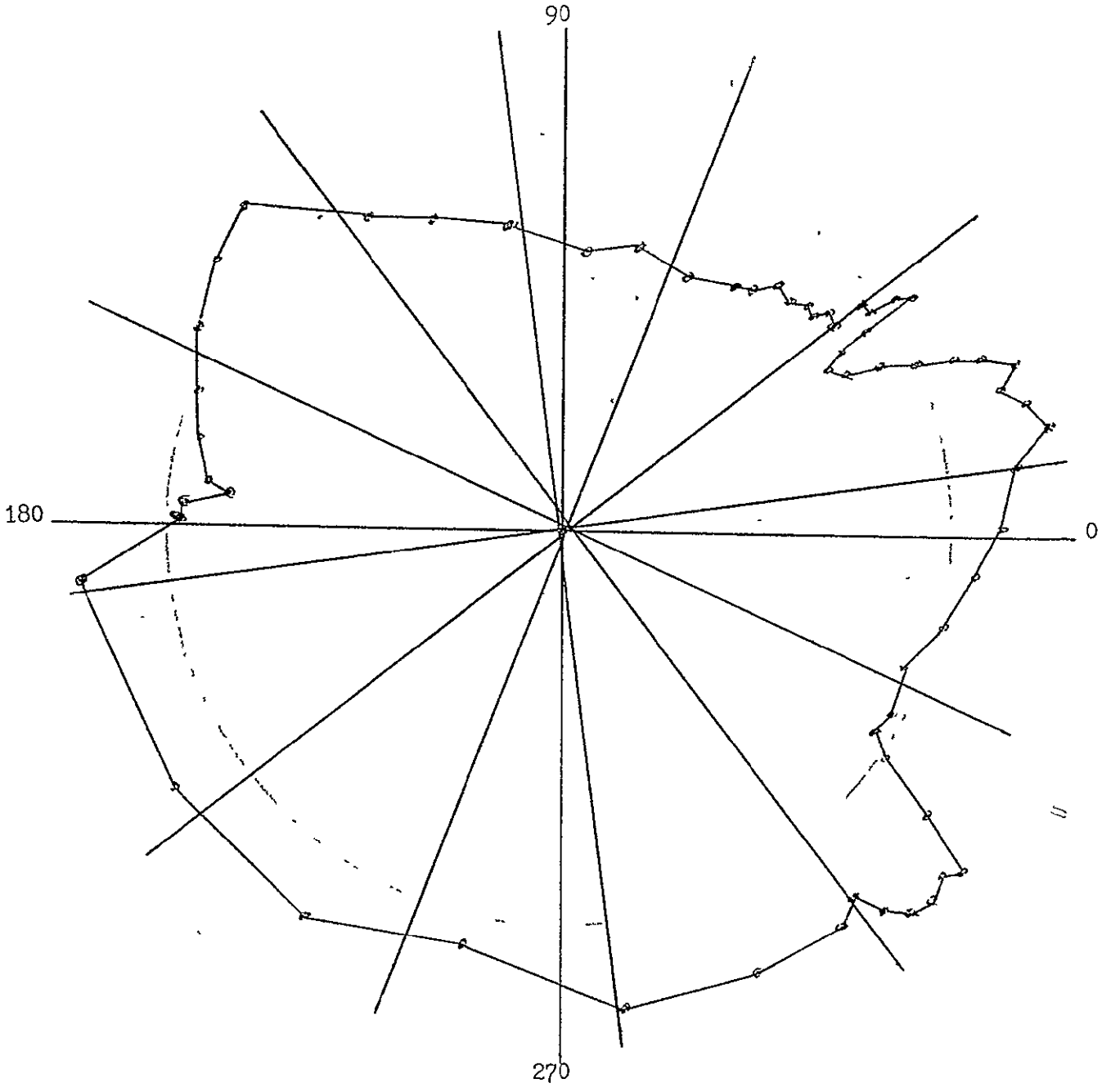


Figure A-5 POLAR PLOT OF INVERSE CORRELATION SLOPE

ORIGINAL PAGE IS
OF POOR QUALITY

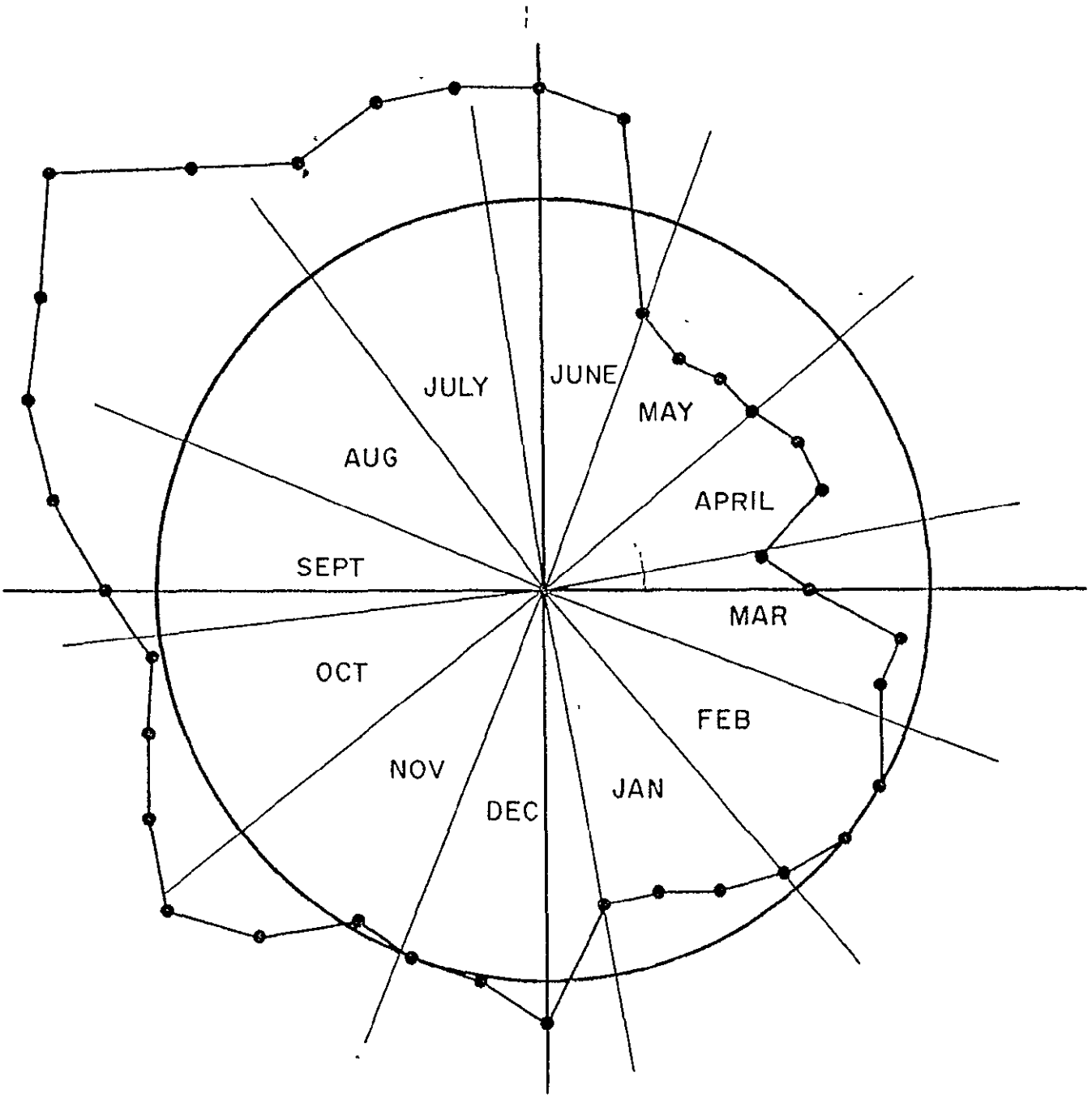


Figure A-6 POLAR PLOT OF EVENING/MORNING RATIOS

APPENDIX B

ON THE INTERSTELLAR DUST TOWARD THE GALACTIC CENTER

ON THE INTERSTELLAR DUST TOWARD THE GALACTIC CENTER

F. E. ROACH
Measurements Analysis Corporation, Boulder, Colorado, U.S.A.

ABSTRACT

Independent observations of two photometric properties of the Milky Way near the direction toward the galactic center are reported. The first is a set of colorimetric measurements from the space satellite OSO-6. The second is a photometric sweep across the Milky Way with a photoelectric photometer attached to the 2.24-meter telescope of the University of Hawaii at the Mauna Kea observatory. The resulting data are: 1) the color index of the region, and 2) its diffuse galactic light. The interrelationship of the observed parameters is discussed with respect to an interstellar-dust component.

I. INTRODUCTION

Direct evidence for a dust concentration in the Milky Way is the presence of obscuring clouds which interrupt its photometric pattern, ranging from the large-scale rifts apparent to the visual observer to small globules which appear to be stars in utero. The obscuration of extra-galactic objects in the vicinity of the Milky Way, the so-called "zone of avoidance", is apparently due to the preferential extinction from this same extensive dusty material.

Four interrelated photometric effects result. 1) the reddening of light that traverses the medium, 2) the scattering of starlight by the material, giving a general diffuse galactic glow, 3) the weakening of light from individual stars viewed through the dusty material, and 4) the polarization of light by irregularly shaped particles that assume some degree of preferential orientation in the interstellar magnetic field. The present study includes the presentation of some observational results on 1) and 2) above, and a discussion of 3), all with respect

to the general region toward the galactic center Since our observational probe pierces only a small fraction of the distance to the galactic center, probably less than 10%, we are interrogating a very small fraction of the total line-of-sight medium in the neighborhood of the constellations Scorpius and Sagittarius.

II. THE COLOR PATTERN

The observational material in our color study is from a colorimeter-photomter-polarimeter on the orbiting solar observatory, OSO-6. The research satellite was launched in August of 1969 and performed steadily until it was "turned off" after about 2-1/2 years and some 13,000 orbits. The details of the equipment and its operation are given in several reports [1]. Here it is pertinent to give the colorimetric data.

Three color filters were brought progressively and systematically into the optical path. The effective wavelengths were not the same as those used by the astronomical fraternity (Table 1). We propose using the astronomical convention of giving colors as "color indices" in stellar magnitude units. Thus, in general,

$$\text{C.I.} = m_2 - m_1 = 2.5 \log \frac{L_1}{L_2} , \quad . \quad . \quad . \quad . \quad . \quad . \quad . \quad . \quad . \quad (1)$$

where m_1 and m_2 are apparent magnitudes in colors 1 and 2 and L_1 and L_2 are the measured brightnesses in the two colors. Because of differences in the filter transmissions and the receiver's sensitivity for the wavelengths in question, any photometric system does not yield directly comparable readings in two color regions. In this study we propose to limit our discussion to the index $b - r^*$. The working formula in that case is

$$b - r = 2\ 5 \log \frac{L_{6100}}{L_{4000}} + 0.952 , \quad . \quad . \quad . \quad . \quad . \quad . \quad . \quad . \quad (2)$$

where the 0.952 has been empirically determined.

---

* Note that we use lower-case symbols to distinguish our results from the conventional astronomical indices.

The observing program on OSO-6 included readings through the color filters for selected elongations with respect to the sun. Some 15 observations in a particular elongation are included in each day (15 orbits per day), and 30 separate readings are included for each orbit. The field of view is 2 degrees in diameter. Since in one day the sun moves, with respect to the celestial background, about 1 degree/ (one half the field of view), we have found it convenient in our working calculations to average the data by calendar day, giving us a total of 15 x 30 = 450 readings entering into the mean for each color-day.

A seven-fold rake across the Milky Way in the general direction toward the galactic center is included in the study, for elongations +195, -170, -175, -180, -185, -190, and -195. The minus elongations refer to "morning" observations when the satellite has just emerged from the terrestrial shadow. The plus elongation refers to "evening" observations just prior to the satellite's reentry into the terrestrial shadow. In Table 2 we have assembled the observational values of $b - r$ ordered according to the galactic latitude of the look direction for each of the seven elongations.

A gross feature of the results is shown in Figure 1, in which the mean values of $b - r$ (for the negative elongations) are plotted against galactic latitudes. Reddening, as evidenced by the increase in $b - r$, is seen to peak at galactic latitude -5°. The observed range is about 0.21 magnitude, corresponding to a 1.213 increase in the ratio of 6100A (red) brightness to that of 4000A (blue) between the lower and upper parts of the curve.

The color pattern from the ensemble of data is shown in Figure 2. The general reddening at about -5° galactic latitude is apparent, but we now note structure in galactic longitude, the maximum reddening occurring at a galactic longitude close to 0°.

THE DIFFUSE GALACTIC LIGHT

The line-of-sight dust that reddens and weakens light which traverses it also scatters radiation that impinges on it from all directions. Thus we have an apparent paradox that a "dark" region in the Milky Way may appear dark by contrast by virtue of the obscuring of stars beyond it but actually may be "bright" as a result of the scattering of light, forward for the starlight which is in the line-of sight but into the observer's eye from the entire sphere of illumination [2].

The discrimination of the diffuse galactic light (DGL) in the totality of light in the Milky Way is a technologically difficult task and the sporadic measurements recorded in the literature have yielded quantitative data for a relatively small fraction of the Milky Way. The direction toward the galactic center is one of particular interest because of the presence of a significant dust constituent in that direction.

A large field such as the 2-degree-diameter field used in the OSO-6 experiment is not ideal for the measurement of the DGL, since a sweep across the Milky Way includes a strong component of direct integrated starlight, the elimination of which introduces uncertainties of calibration and of star-count statistics. To use a small field it is necessary, in order to have a measurable flux onto the cathode of a photoelectric receiver, to employ a large-aperture telescope. Such a small field permits the observer to scan across the Milky Way between all but the faintest of the stars.

In 1971 I made a sweep across the Milky Way with a field of only 26-arcsecond diameter. The University of Hawaii telescope of 2.24-meter aperture was employed, using the sliding-field technique in which the telescope, set at a declination of $-23^{\circ}29'$, was not driven, successive sky elements traversing the field as a result of the earth's rotation. In a previous use of this method [3], the successive readings were digitized. In the present study an analogue record was obtained.

As individual stars entered the field, spikes appeared on the record. The "background" was estimated by connecting the low readings for each degree of right ascension.

The slice of the Milky Way included in this study paralleled very closely the color slice of the OSO-6 data for elongation -180° as discussed in the previous section of this report. The small field used resulted in a rather small component of direct integrated starlight included in the background readings (compare with figure 5 in reference [3]). The slice did include a significant amount of zodiacal light/gegenschein, which was subtracted from the working data. Also a small amount of airglow ~~seemed to~~ gave a further contaminant.

The final estimate of the DGL from the Mauna Kea observations is shown in column 2 of Table 3. For direct comparison, the values of $b - r$ for the -180° sweep of OSO-6 (column 5 of Table 2) are repeated. In Figure 3 we show the DGL and $b - r$, each plotted against galactic latitude. A similarity in the two patterns, ~~so that an index (x) and diffuse galactic light~~ is obvious. An increase in the DGL occurs in reddened regions. A dip in the DGL near the galactic equa-or corresponds to a dip in the reddening curve. Thus the evidence supports the hypothesis that the same line-of-sight material scatters and reddens the light which impinges on it.

In Figure 4 we show a plot of observed DGL versus $b - r$ (from Table 3). Since the $b - r$ is by nature logarithmic and the DGL linear, a least-squares relationship between them was obtained by a working plot of a logarithmic function of DGL versus $b - r$, which yielded the following relationship

$$\text{DGL} = 10 \exp [4\ 819\ (b' - r) - 3.475] \quad . \quad . \quad . \quad . \quad . \quad . \quad . \quad (3)$$

(correlation coefficient, 0.766). This analytical curve is shown in Figure 3 for comparison with the observations.

THE TOTAL ABSORPTION

The effective distance to the "dusty" cloud responsible for the observed color and scattering effects discussed in this paper is not known, but a rough estimate results from the fact that the peak of light from the stars in the Milky Way in general is due to stars of apparent visual magnitude about 13. If we take the peak of luminosity contribution to be from stars of absolute visual magnitude 5, then, in the absence of interstellar absorption,

$$m - M = 13 - 5 = 8 = 5 \log r/10 \quad . \quad . \quad . \quad . \quad . \quad . \quad . \quad . \quad (4)$$

where the effective distance, r, to the center of the cloud is 398 parsecs. Any significant absorption will reduce this distance estimate. If the peak of the flux contribution is from fainter stars than $m_v = 13$, the deduced distance to the ensemble of stars is increased; for example, if $m_v = 14$, $r = 631$ parsecs for the case of no interstellar absorption. The dusty region is probably closer to the sun than the line-of-sight stars. It is interesting to note that the likely distance to the general dusty cloud thus brackets at distances similar to those determined for discrete globules [4].

A copious literature deals with the interrelationship between reddening of individual stars and their total absorption in the Milky Way. The type of surface photometry under study in this paper is inherently different from the photometry of individual stars, since we are here dealing with an integrated reddening and scattering along the line of sight. However, it is of some interest to make a star-parallel study of the parameters of our surface photometry In that spirit, we have made working calculations of the effective total absorption from the observed $b - r$ by

$$A_v = 2.2 \; E_{(b-r)} \quad . \quad . \quad . \quad . \quad . \quad . \quad . \quad . \quad . \quad . \quad . \quad . \quad (5)$$

where A_v is the total visual absorption in stellar magnitudes and $E_{(b-r)}$ is the color excess in our $b - r$ system. Outside the Milky Way the general value of $b - r$ is 0.98, whence

$$A_v = 2.2\ [(b - r) - 0.98]$$

$$= 2.2\ (b - r) - 2.156 \quad . \quad . \quad . \quad . \quad . \quad . \quad . \quad . \quad . \quad . \quad (6)$$

The extinction due to this absorption is

$$e^{-\tau} = 10 \exp\ (-0.4\ A_v)$$

$$= 10 \exp\ [-0.88\ (b - r) + 0.862]$$

where τ is the optical thickness.

In a simplified treatment of the scattering leading to the DGL, the scattered light is proportional to $(1 - e^{-\tau})$. In Table 3 we have tabulated Av computed from Eq. (5), $e^{-\tau}$ from Eq. (6), $1 - e^{-\tau}$ and the quantity $\Phi = DGL/(1 - e^{-\tau})$. The quantity Φ is plotted for our observations versus $b - r$ together with a smooth curve derived from a combination of the earlier equations in Figure 5.

$$\Phi \simeq \frac{DGL}{1-e^{-\tau}} = \frac{10 \exp\ [4.819\ (b - r) - 3.475]}{1 - 10 \exp\ [-0.88\ (b - r) + 0.862]} \quad . \quad . \quad . \quad (8)$$

The physical interpretation of Figure 4 is involved with the factor of proportionality in

$$DGL = K\ (1 - e^{-\tau}) \quad . \quad . \quad . \quad . \quad . \quad . \quad . \quad . \quad . \quad . \quad . \quad (9)$$

$(= \Phi)$

K includes the spherical albedo of the particles and the total light from the sphere surrounding the dust milieu. The scattering phase function is also involved in the general relationship. The quantity Φ is greater than the directly observed line-of-sight starlight in four regions (Figure 6). A comparison with the rather crude estimates of direct starlight by Roach and Megill [5] in the domain of the traverses of this paper gives

$$\Phi \simeq 1.4(RM \times e^{\tau}) \quad . \quad . \quad . \quad . \quad . \quad . \quad . \quad . \quad . \quad . \quad (10)$$

where the RM interpolated values have been multiplied by e^{τ} (column 8, Table 3), to convert same to the values on the far side of the dust sheet. Since the spherical albedo of the particles is probably less than unity, it would appear that Φ

is a lower limit of the total brightness of the starlight that impinges on the dust sheet. Of interest is the region from galactic latitudes -3° to -10° We have already noted that this is a domain of large color excess in $b - r$ and large DGL. The implication of our analysis is that the total light irradiating the dust in this direction is as much as two times the directly transmitted light in the line of sight. However, the fact that Φ and $RM \times e^{\tau}$ are approximately equal over a fraction of the sweep across the Milky Way is consistent with a phase function that is significantly forward-scattering.

SUMMARY

An attempt is made to discuss the interrelationship among the photometric parameters in the general direction toward the galactic center. Measurements of the reddening of the light are based on observations from the OSO-6 satellite. The diffuse galactic light for a slice through the reddening domain is estimated from ground observations at the University of Hawaii observatory on Mauna Kea. Finally, the amount of the irradiation on the dusty sheet is estimated on an assumed relationship among the reddening, the scattering (DGL), and the total absorption in the line of sight.

ACKNOWLEDGMENT:

This study was supported by NASA Contract NASW-2902.

REFERENCES

1. Ball Brothers, "Rutgers Zodiacal Light Analyzer for OSO-G. Final Report F70-11. 1970.

2. Struve, O., *Astrophysical Journal, 85*, 194, 1937.

3. Roach, F.E., J. Pfleiderer, C. Batishko, and K. Batishko, *Astrophysical Journal, 173*, 343, 1972.

4. Bok, B.J., in his Bruce Medalist lecture presented to the Astronomical Society of the Pacific in 1977, gave a general summary of globules including their distances. To be published in *P.A.S.P.*

5. Roach, F.E., and L.R. Megill, *Astrophysical Journal, 133*, 228, 1961; see also Megill and Roach, NBS Technical Note No. 106, 1961.

LEGENDS FOR FIGURES:

Figure 1. Mean Value of $b - r$ Plotted Versus the Galactic Latitude; from Columns 1 and 9, Table 2. Plus and 1 1 sigma (standard deviation of the mean) from column 10 is indicated by the vertical extensions.

Figure 2. Isocolor ($b - r$) Map in Galactic Latitude and Galactic Longitude, from Table 2.

Figure 3. The Diffuse Galactic Light (DGL) from Observations at Mauna Kea and the Corresponding Color Index ($b - r$) from OSO-6 Plotted against Galactic Latitude. From columns 1, 2, and 3 of Table 3.

Figure 4. Diffuse Galactic Light Versus $b - r$ from Columns 2 and 3 of Table 3. The line is a plot of Eq. 3 (see text).

Figure 5. DGL/1 - $e^{-\tau}$ Versus $b - r$ from Columns 7 and 3 of Table 3. The line is a plot of Eq. 8 (see text).

Figure 6. The Quantity Φ (Ratio DGL/1 - $e^{-\tau}$) and the Directly Observed Integrated Starlight from Roach and Megill [5] Plotted Against Galactic Latitude. The *RM* values have been multiplied by e^{τ} to give estimated values on the "far side" of the scattering region.

Table 1. Comparison of OSO-6 Color System with the Standard UBV System

Astronomical Standard	OSO-6	Peak Wavelength (A)	
U	b	3500	4000
B	v	4400	5000
V	r	5500	6100
R		7000	

Table 2. Observed Color Index, $b - r$

b	Elongation, ε							Mean*	σ_{mean}
	+195	-170	-175	-180	-185	-190	-195		
10		1.094	1.158	1.097	1.087	1.079	1.010	1.087	0.047
9		1.146	1.119	1.115	1.120	1.045	1.006	1.092	.054
8		1.124	1.118	1.120	1.148	1.057	1.103	1.112	.030
7		1.111	1.125	1.080	1.139	1.109	1.089	1.109	.022
6		1.143	1.135	1 134	1.169	1.121	1.030	1.122	.048
5		1.136	1.127	1.195	1.174	1.093	1.027	1.125	.060
4		1.101	1.183	1.252	1.177	1.083	1.068	1.144	.072
3	1.031	1.071	1.200	1.265	1.161	1.080	1.046	1.137	.086
2	1.045	1.109	1.214	1.238	1.127	1.070	1.087	1.141	.069
1	1.050	1.117	1.131	1.235	1.097	1.080	1.069	1.121	.060
0	1.070	1.132	1.228	1.094	1.242	1.122	1.041	1.143	.078
-1	(1.080)†	1.157	1.238	1.054	1.049	1.156	1.162	1.136	.072
-2	(1.098)	1.204	1.299	1.179	1.110	1.174	1.221	1.198	.062
-3	(1.118)	1.318	1.317	1.258	1.178	1.186	1.206	1.244	.064
-4	(1.135)	1.349	1.318	1.289	1.196	1.189	1.221	1.260	.068
-5	1.176	1.360	1.326	1.278	1.188	1.200	1.190	1.257	.075
-6	1.210	1.356	1.288	1.257	1.246	1.210	1.157	1.252	.068
-7	1.180	1.276	1.285	1.234	1.196	1.152	1.122	1.211	.066
-8	1.128	1.225	1.242	1.212	1.156	1.113	1.083	1.172	.065
-9	1.104	1.095	1.224	1.200	1.122	1.085	1.128	1.142	.057
-10	1.050	0.998	1.224	1.194	1.109	1.106	1.116	1.124	.079
-11	0.972	1.103	1.212	1.149	1.103	1.112	1.103	1.130	.044
-12	0.990	1.131	1.056	1.131	1.074	1.098	1.093	1.097	.030
-13	0.975	1.115	1.022	1.110	1.073	1.096	1.091	1.084	.034
-14	0.982	1.101	0.863	1.106	1.081	1.092	1.038	1.047	.093
-15	0.962	1.062	1.002	1.042	1.008	1.106	1.073	1.049	040

*Mean is of the six negative elongations only.

†Values in parentheses are uncertain because of full moon.

ORIGINAL PAGE IS
OF POOR QUALITY

ORIGINAL PAGE IS
OF POOR QUALITY

Table 3. Diffuse Galactic Light Observed at Mauna Kea

b^{II} (deg)	DGL	$b - r$	Av	$e^{-\tau}$	$1 - e^{-\tau}$	$\frac{DGL}{1 - e^{-\tau}}$	$RM \times e^{\tau}$
10	106	1.097	0.257	0.789	0.211	502	188
9	65	1.115	.297	.761	.239	272	208
8	114	1.120	.308	.753	.247	462	219
7	168	1.080	.220	817	.183	918	219
6	120	1.134	.339	.732	.268	448	258
5	114	1.195	.473	.647	.353	323	308
4	140	1.252	.598	.577	.423	331	541
3	240	1.265	.627	.561	.439	547	590
2	265	1.238	.568	.593	.407	651	486
1	122	1.235	.561	.596	.404	302	529
0	98	1.094	.251	.794	.206	476	435
-1	180	1.054	.163	.861	.139	1295	426
-2	144	1.179	.438	.668	.332	434	552
-3	275	.1258	.612	.569	.431	638	606
-4	450	1.289	.680	.535	.465	968	594
-5	455	1.278	.656	.547	.453	1004	541
-6	308	1.257	.609	.571	.429	718	496
-7	335	1.234	.559	.598	.402	833	452
-8	264	1.212	.510	.625	.375	704	414
-9	208	1.200	.484	.640	.360	578	389
-10	136	1.194	.471	.648	.352	386	369
-11	98	1.149	.372	.710	.290	338	330
-12	144	1.131	.332	.737	.263	548	308
-13	75	1.110	.286	.768	.232	323	288
-14	64	1.106	.277	.775	.225	284	277
-15	30	1.042	.136	.882	.118	254	237

Source: See Text | $\varepsilon=-180^{o}$ Table 2 | Eq. 5 | Eq. 7 | Eq. 8

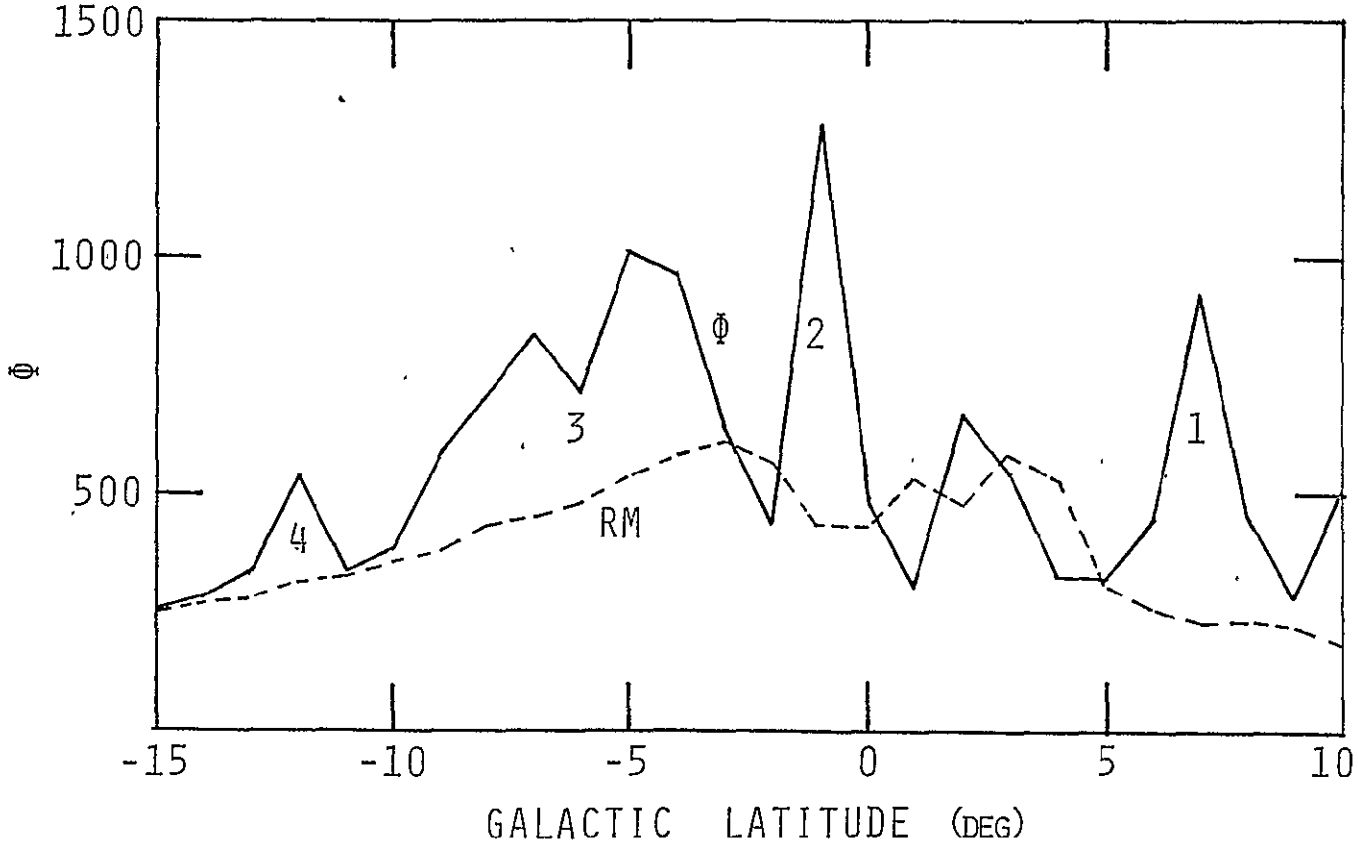


Figure B-1 MEAN VALUE OF b-r index VERSUS GALACTIC LATITUDE

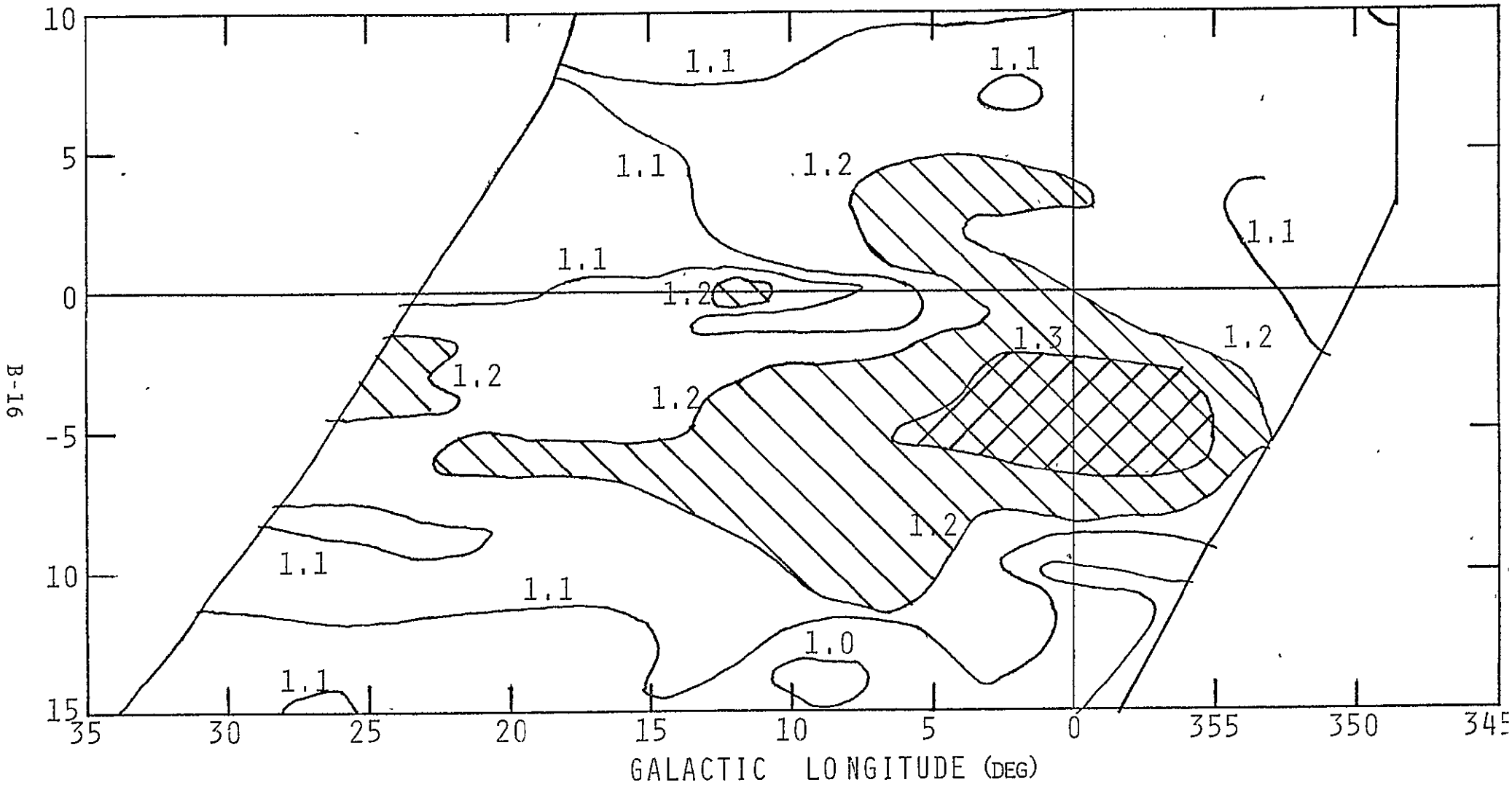


Figure B-2 ISOCOLOR MAP IN GALACTIC LATITUDE AND LONGITUDE

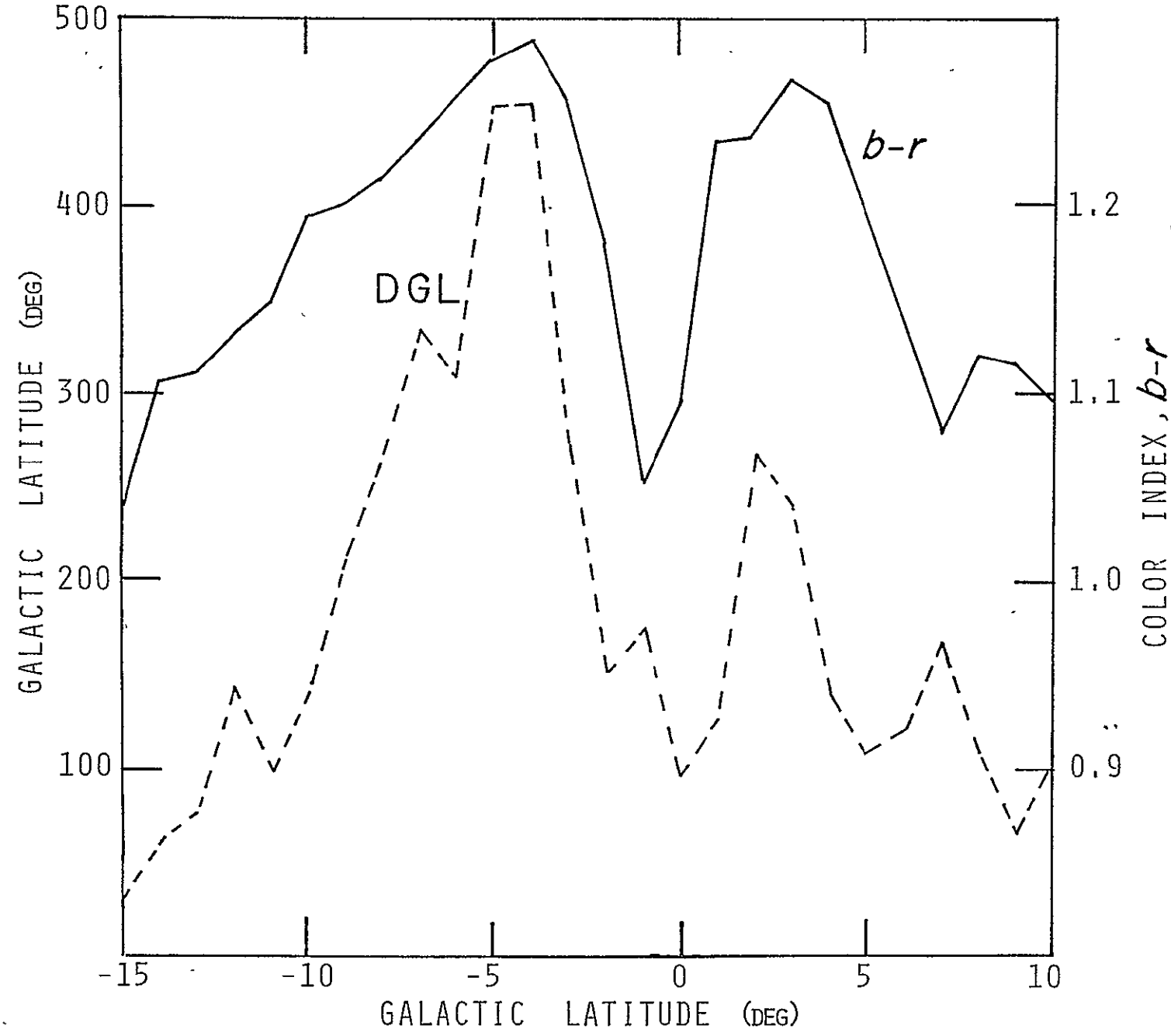


Figure B-3 MAUNA KEA DIFFUSE GALACTIC LIGHT AND OSO-6 COLOR INDEX VERSUS GALACTIC LATITUDE

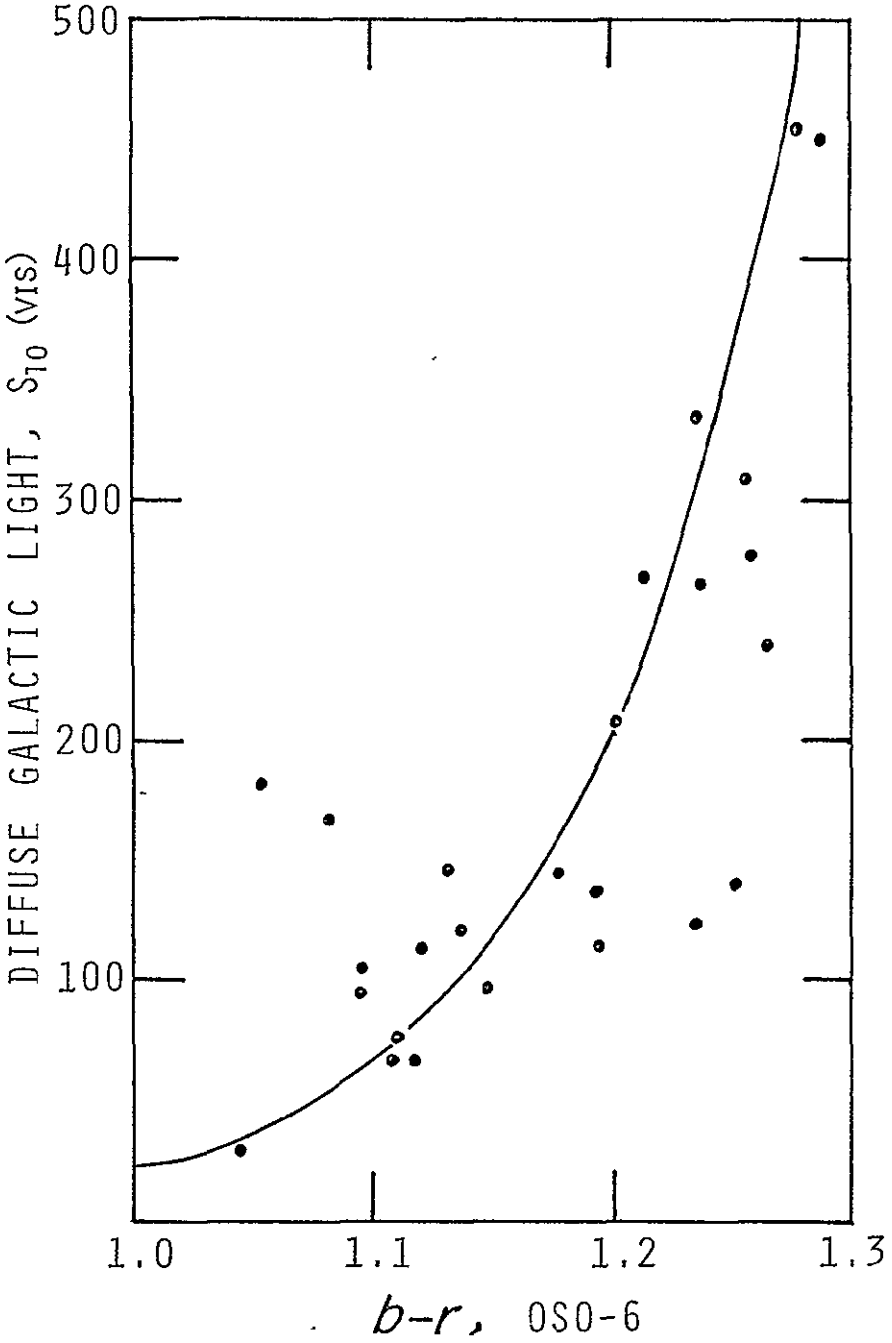


Figure B-4 DIFFUSE GALACTIC LIGHT VERSUS OSO-6 b-r INDEX

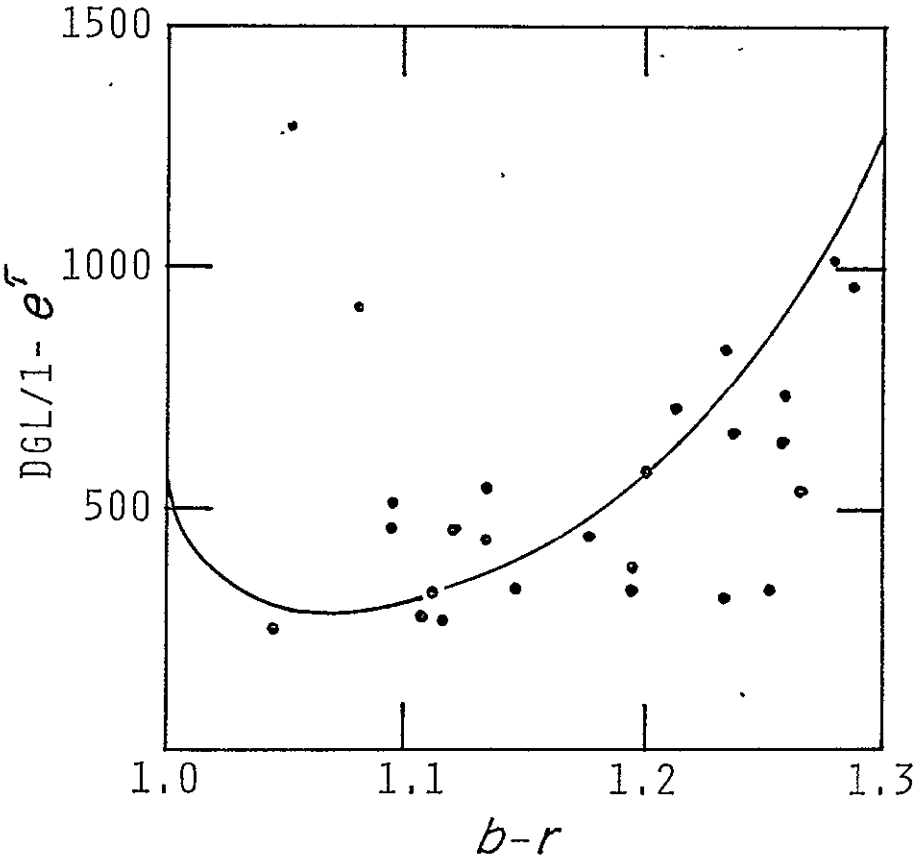


Figure B-5 DIFFUSE GALACTIC LIGHT INDEX VERSUS OSO-6 b-r INDEX

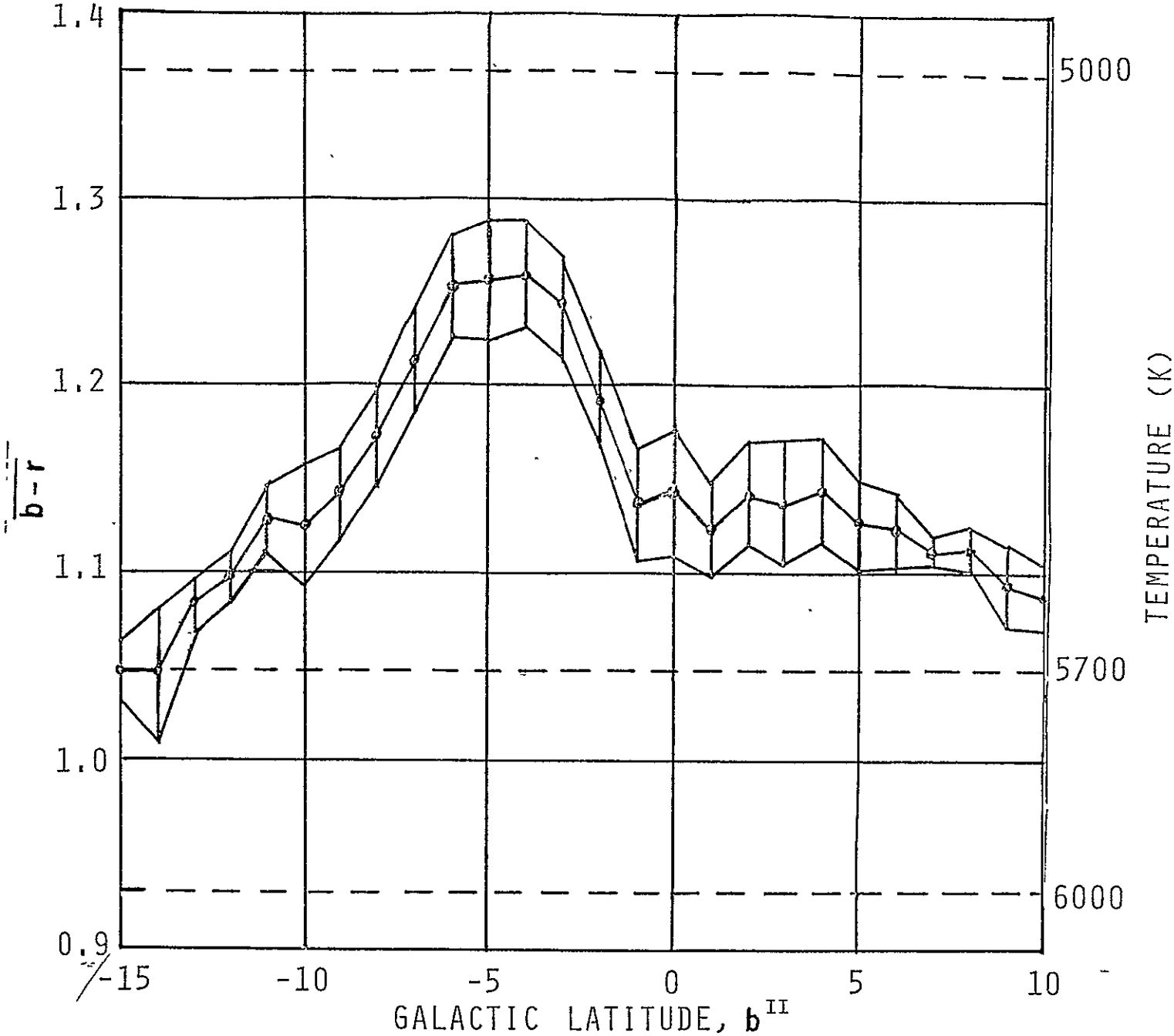


Figure B-6 THE QUANTITY $\overline{b-r}$ AND INTEGRATED STARLIGHT VERSUS GALACTIC LATITUDE

APPENDIX C

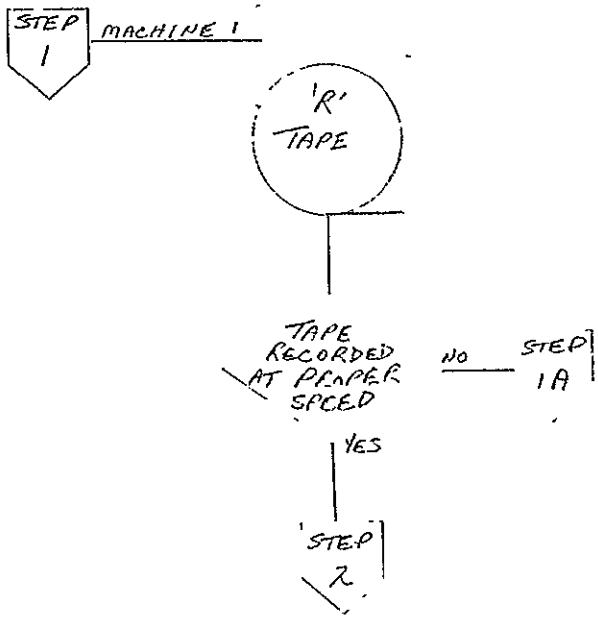
DATA PROCESSING FUNCTIONAL FLOW AND SOFTWARE PROGRAMS

OSO-6 ZODIACAL LIGHT EXPERIMENT

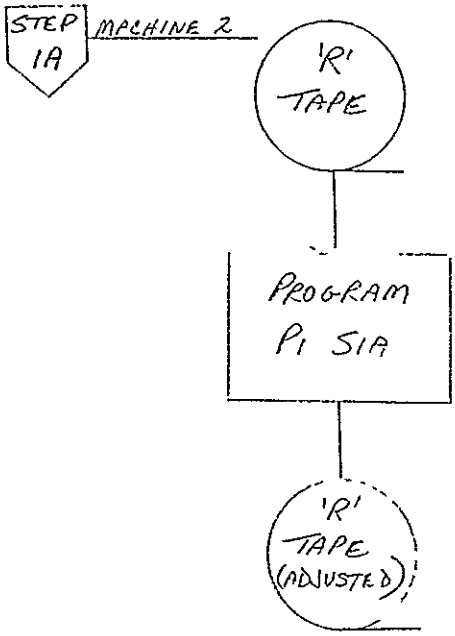
DATA PROCESSING FLOW

ORIGINAL PAGE IS
OF POOR QUALITY

PASS 1

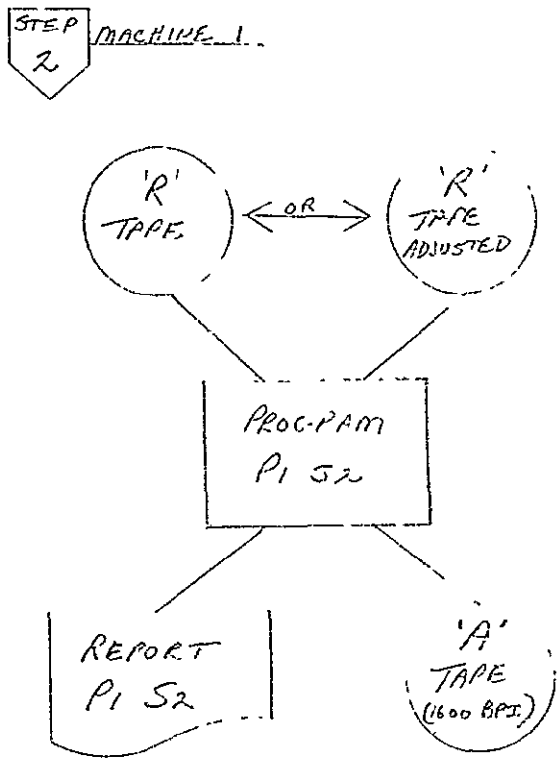


'R' Tape - NASA Raw Data Tapes (7 track)



Program P1 S1A. Adjusts for variable tape speeds.

ORIGINAL PAGE IS
OF POOR QUALITY

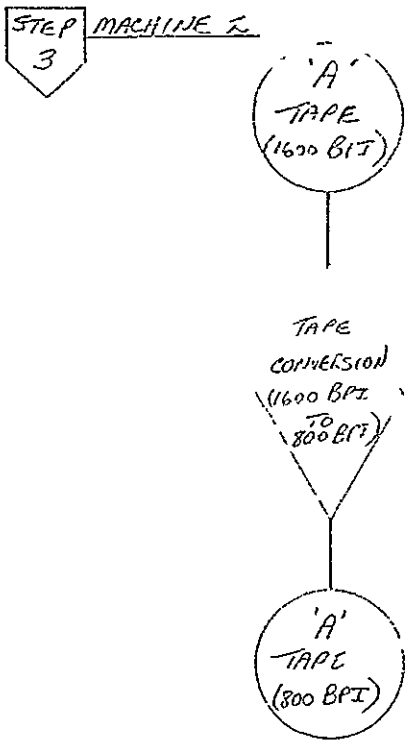


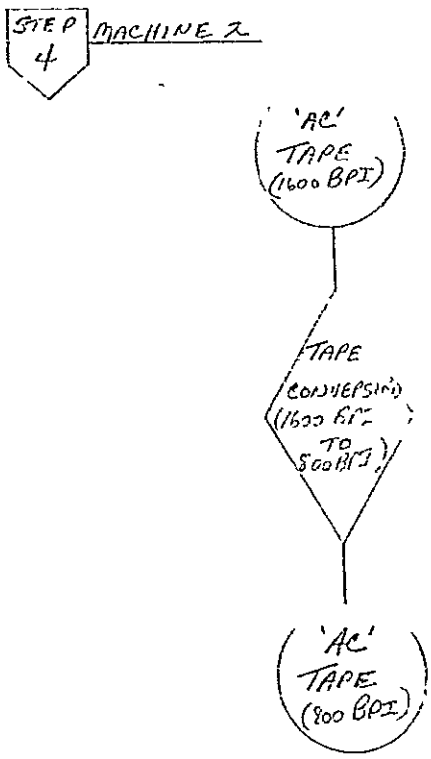
Program P1 S2. Process per Orbit per Elongation Angle (12)

- Establishes internal sync
- Obtains Avg. hub temp.
- Demultiplexes Internal format

Report P1 S2.

- No. of good data words per set
- Avg. hub temp.

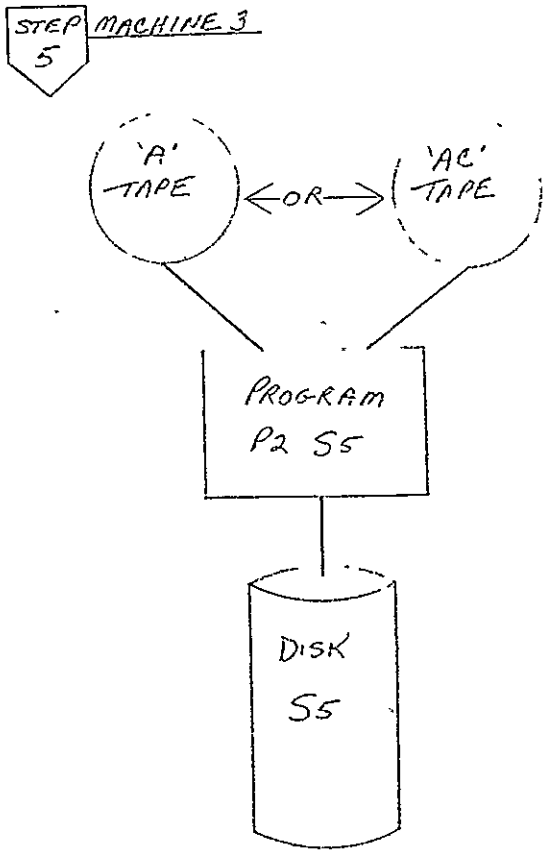




'AC' Tape. Previously processed data.

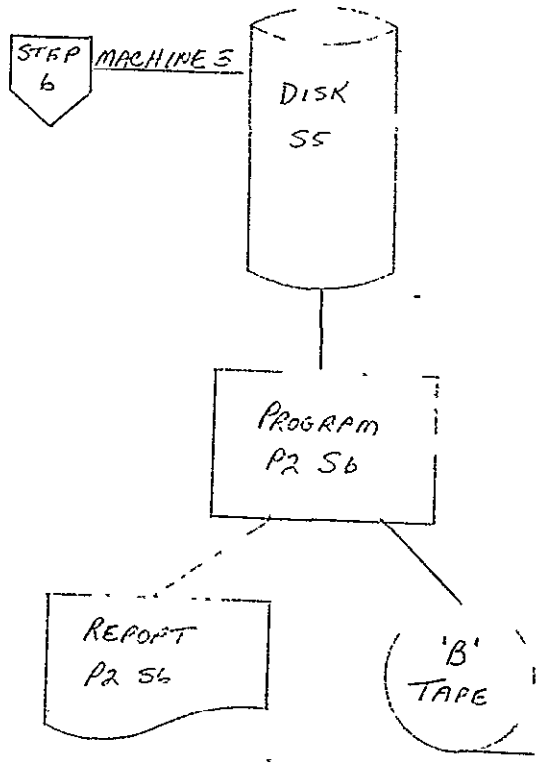
ORIGINAL PAGE IS
OF POOR QUALITY

PASS 2



Program P2 S5. Copies Tape to Disk.

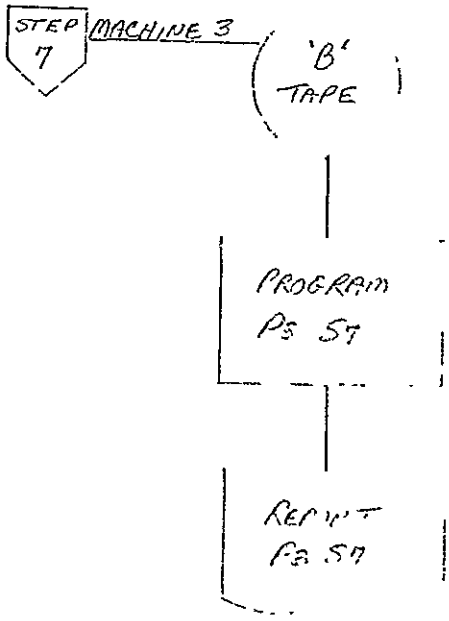
ORIGINAL PAGE IS
OF POOR QUALITY



Program P2 S6. Process per Orbit:
- Converts internal offset TM count to continuous count
- Calculates Temp. correction
- Linearizes data count
- Applies dark current correction
- Purges out of tolerance data
- Determines elongation angle
- Averages per polarization setting
- Averages per color band

Report P2 S6. Prints per Orbit:
Option 1: All Data
Option 2: Grand Averages
- Raw Data
- Linear Data

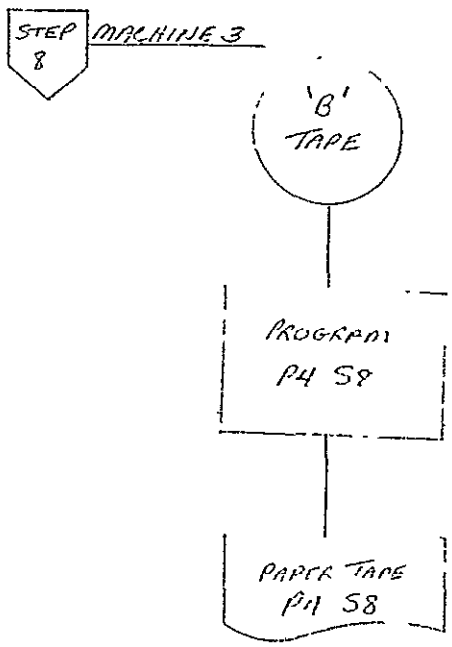
PASS 3



Program P3 S7. Process Per Orbit:
- Calculates Color Indices (3)
- Calculates Sky Temperatures (4)

Report P3 S7. Prints Per Orbit Per Elongation Angle (12)
- Linear Grand Averages
- Color Indices
- Sky Temperatures
- Observation Mode
- Temperature Correction
- Day of Year
- Time of Day

PASS 4



Program P4 S8. Process Per Orbit:
- Calculates Color Indices (3)
- Calculates Sky Temperatures (4)

Paper Tape P4 S8. Per Orbit Per Elongation Angle (12)

Option 1:
- Raw Data Grand Averages (3)
- Linear Data Grand Averages (3)
- Observation Mode
- Temperature Correction

Option 2:
- Linear Data Grand Averages (3)
- Color Indices (3)
- Sky Temperatures (4)
- Observation Mode
- Temperature Correction
- Day of Year
- Time of Day